Digitized Theses   Digitized Special Collections

2008

Non-Invasive Assessment of Disease Progression in Transgenic Murine Models of Duchenne Muscular Dystrophy

Nabeel Ahmad
Western University

Follow this and additional works at: https://ir.lib.uwo.ca/digitizedtheses

Non-Invasive Assessment of Disease Progression in Transgenic Murine Models of Duchenne Muscular Dystrophy

(Spine Title: Multi-modal Imaging of Disease Progression in Models of DMD)
(Thesis Format: Integrated Article)

by

Nabeel <u>Ahmad</u>

Graduate Program
in
Medical Biophysics

Submitted in partial fulfillment
of the requirements for the degree of
Master of Science

School of Graduate and Postdoctoral Studies
The University of Western Ontario
London, Ontario, Canada

THE UNIVERSITY OF WESTERN ONTARIO
School of Graduate and Postdoctoral Studies

CERTIFICATE OF EXAMINATION

SUPERVISOR	*EXAMINERS*
Dr. Ting-Yim Lee	Dr. Dan Goldman
SUPERVISORY COMMITTEE	Dr. Terry Thompson
Dr. Savita Dhavantari	Dr. Cesare Romagnoli
Dr. Ian Welch	

The thesis by

Nabeel Ahmad

entitled:

Non-invasive Assessment of Disease Progression in Transgenic Murine Models of
Duchenne Muscular Dystrophy

is accepted in partial fulfilment of the
requirements for the degree of
Master of Science

_____   _____
Date   Chair of the Thesis Examination Board

ABSTRACT

Introduction: Duchenne muscular dystrophy (DMD) is a severe X-linked neuromuscular disease which arises from the mutation of the cytoskeletal structural protein, dystrophin. Currently, no established non-invasive method exists to assess disease progression.   In the present study we have used dynamic contrast-enhanced computed tomography (DCE-CT), positron emission tomography (PET) and high frequency ultrasound (HFU) imaging to non-invasively measure changes in muscle perfusion, metabolism and architecture starting at 6 weeks of age for 16 weeks in two dystrophic murine models, mdx (mutated dystrophin) and udx (mdx:utrophin-null).

Methods: Mice were divided into 4 groups by genotype and exercise treatment to induce muscle damage: (1) wild-type (wt)-run, (2) mutated dystrophin (mdx)-run, (3) mdx-walk, and (4) mdx/utrophin-null (udx)-walk. All mice in the 'run' groups were exercised on a motorized treadmill at a speed of 15 meters per minute (mpm) and a 7-degree incline for 30 minutes, 3 times weekly from 6 to 22 weeks of age.   All 'walk' mice followed the same exercise regime but walked for 10 minutes at 5–7 mpm with no incline. Mice were imaged at baseline, imaging was then bi-weekly after exercise sessions with DCE-CT, FDG-PET and HFU to measure gastrocnemius muscle blood flow (BF) and volume (BV), ^{18}F-FDG uptake (metabolism) as standardized uptake value (SUV) and to grade skeletal musculature changes using HFU.

Results: Mean gastrocnemius blood flow in udx and mdx mice peaked at 8 weeks of age and was 40% and 35% higher ($p < 0.05$), respectively, than baseline or those for wt mice. Udx and mdx mice at early post exercise had 55% and 20% higher SUV

(p<0.05), respectively, than wt mice. Initial increases in BF, BV and SUV were followed by a slow decline with increased duration post exercise. HFU discriminated the severity of muscle damage between wt and dystrophic models, as well as between the mdx and udx dystrophic models. Udx mice displayed continual increase in muscle damage throughout the study. Mdx mice (Ex, N.E) displayed an initial increase in muscle damage followed by reduced degeneration till 22 weeks of age.

Conclusion: The patterns of changes in imaging parameters are consistent with initial muscle de/regeneration, inflammation and subsequent muscle necrosis seen in histology. Imaging was capable of differentiating between wild type and affected animals as an non-invasive assessment of disease progression.

Keywords: Duchenne Muscular Dystrophy, Murine, Perfusion, Metabolism, Computed Tomography, Positron Emission Tomography, High Frequency Ultrasound

EPIGRAPH

"The world is composed of three days. As for yesterday, it has vanished. As for tomorrow, you may never see it. As for today, it is yours, so make the most of it."

-Hassan Al-Basri

"Education is the passport to the future, for tomorrow belongs to those who prepare for it today."

-Malcolm X

CO-AUTHORSHIP

Chapter 2 has been adapted from the paper entitled "Functional Imaging of Disease Progression in Murine Models of Duchenne Muscular Dystrophy", submitted to Molecular Imaging in 2008, by Nabeel Ahmad, Lisa Hoffman, Ian Welch, Robert Grange, Jennifer Hadway, Savita Dhanvantari, Rethy Chemm, David Hill and Ting-Yim Lee. I was responsible for designing the study, performing experiments, collecting and analyzing data, histopathology and writing the manuscript. Ting-Yim Lee was responsible for project concepts, provided supervision and reviewed the manuscript. Lisa Hoffman provided project concepts, helped with PET scans and reviewed the manuscript. Ian Welch assisted with reviewing and analyzing histopathology. Jennifer Hadway assisted with the development of the animal protocol and was responsible for animal transportation, scanning and care. Remaining authors helped with editing the manuscript.

Chapter 3 has been adapted from the paper entitled "High frequency ultrasound as a non-invasive tool to assess disease progression in murine models of Duchenne Muscular Dystrophy" submitted to Journal of Ultrasound in Medicine in November 2008, by Nabeel Ahmad, Mike Bygrave, Rethy Chemm, Ian Welch, Lisa Hoffman, Robert Grange, Ting-Yim Lee. I was responsible for designing the study, performing experiments, collecting and analyzing data, histopathology and writing the manuscript. Mike Bygrave scanned the animals, assisted in scan analysis and edited the manuscript. Rethy Chemm assisted with the study design. Ting-Yim Lee was responsible for project concepts, provided supervision and reviewed the manuscript. Ian Welch assisted with reviewing and analyzing histopathology. Remaining authors helped with editing the manuscript.

ACKNOWLEDGEMENTS

TABLE OF CONTENTS

CHAPTER 4: CONCLUSIONS AND FUTURE WORK

LIST OF FIGURES

APPENDIX / ETHICS APPROVAL

LIST OF ABBREVIATIONS

ACh   Acetycholine

AIF   Arterial Input Function

BF   Blood Flow

BV   Blood Volume

Ca^{2+} Calcium

CK   Creatine kinase

CSA   Cross sectional areas

CTP   Computed Tomography Perfusion

DCE-CT   Dynamic Contrast Enhanced Computed Tomography

DGC   Dystrophin-glycoprotein complex

DMD   Duchenne Muscular Dystrophy

eNOS   Endothelial NOS

Ex   Exercise

FDG ^{18}Fluro-2-deoxy-D-glucose

GEHC   General Electric Health Care

HFU   High Frequency Ultrasound

iNOS   Inducible NOS

IRF   Impulse Residue Function

MRI   Magnetic Resonance Imaging

NBF   Normalized blood flow

NBV   Normalized blood volume

N.E	Non-exercise
nNOS	Neuronal NOS
NOS	Nitric Oxide
NSUV	Normalized Standard uptake value
PET	Positron Emission Tomography
SPECT	Single Photon Computed Tomography
TDC	Time-Density Curve
US	Ultrasound

CHAPTER 1
INTRODUCTION TO DUCHENNE MUSCULAR DYSTROPHY

1.0   INTRODUCTION

Muscular dystrophy is a devastating genetic muscle disorder, which affects approximately every one in 3500 live male births. The muscular dystrophies represent some of the most frequent and severe disorders following Mendelian inheritance. However, the term "muscular dystrophy" has many different subcategories, which vary in global weakness, severity and muscle groups affected.[1] Often, there are varying degrees of muscle wasting and levels of atrophy, which can be difficult to diagnose due to an accumulation of fat and connective fibrotic tissue.[2] Thus, muscular dystrophy is used as a broad term that describes a group of more than 30 different types of muscle disorders. Of these 30 muscle disorders, Duchenne is the most severe form of muscular dystrophy and the disease type of interest for this study.

Duchenne Muscular Dystrophy (DMD) is characterized by progressive skeletal muscle weakness due to contraction induced muscle damage.[3] The increased induction of muscle damage is caused by an absence or defect in the structural protein dystrophin, which is found in a variety of tissues most notably skeletal muscle.[4] These disruptions cause structural damage within muscle architecture which in turn cause death of muscle cells and tissue.[5]

DMD was the first class of muscular dystrophy to be clearly recognized, and was first termed "pseudo-hypertrophic muscular paralysis". This was due to pronounced hypertrophic growth and deterioration of function of the lower-limb muscles at the time of its discovery. However in 1868, a physician named Guillame Duchenne, documented

and published his results based on clinical descriptions of electrophysiology and muscle histology.[6] His experiments and observations noted that DMD patients presenting symptoms of the disease were males under the age of 20, who developed enlarged, but weakened lower limb muscles and died young usually from respiratory failure.[2,7] Guillame's histology revealed atrophic muscle fibers with progressive interstitial fibrosis and regions of necrosis and regeneration in affected patients.[2]

Since then the phenotypic development of DMD has been well documented. Affected neonates outwardly appear healthy; and a normal course is common throughout the first year of life. However, after the age of one weakening of the voluntary muscles within the pelvic girdle, thigh and calf are seen.[8] Motor delays are another important feature; over half fail to walk alone by 18 months.[9,10] As well extremely elevated serum levels of creatine kinase ranging from 5,000-150,000 IU/L, are found in DMD boys compared to normal levels of <200 IU/L.[11] As walking becomes established, features suggestive of muscle weakness such as an abnormal gait, and clumsiness become apparent. By age five a classic manoeuvre documented by the English neurologist Sir William Richard Gowers is seen.[12] Within a few years, lordosis results from weakness of hip extensors,[13] which further affects the gait of DMD patients consequently increasing the numbers of falls and injuries incurred.[14] Muscle shortening occurs due to fibrosis replacement of muscle tissue, causing contractures and pain.[15] Muscles such as the gastrocnemius begin to display a doughy, pseudo-hypertrophic state due to fat and collagen infiltrate.[14] As the boys reach their early teens severe weakness is seen in the arms and shoulders, with increasing severity, such that even standing by the use of "Gowers sign" or any form of ambulation becomes nearly impossible, as a result most

boys at this age become wheelchair bound.[11] DMD patients are currently prescribed multiple treatments in order to delay disease progression, none of which are curative. Therefore, by better understanding the genetic deficiencies and natural progression of disease we will be able to better address a cure.

1.1 DIAGNOSTIC INVESTIGATION

While diagnosis of DMD is usually made by family history and PCR genotyping, analysis of disease progression typically relies upon the measurement of strength, creatine kinase levels [16] and invasive muscle biopsy assessment.[17] Once diagnosed with DMD multiple treatments and therapies are available in order to help patients cope with the rapid progressive nature of the disease. Clinically, there is no effective means to reliably and non-invasively assess the progression of muscle wasting in DMD, nor the efficacy of various therapies to treat the disease and improve the quality of life for patients.

1.2 CLINICAL TREATMENTS

Since no cure for DMD currently exists, clinicians are left to combat disease progression with the use of drug therapies, physiotherapy, custom made braces with knee-ankle-foot orthoses,[18] and corrective orthopedic surgery and spinal surgery in order to relieve pain and prolong the period of independent ambulation.[19] However, typically by the age of 11 most DMD patients have lost all ambulation and are confined to wheel chairs. At this age respiratory muscles begin to display signs of failure, requiring most patients to use respirators.[20] [21] Clinical tests have shown that ventilators in conjunction with electric wheel chairs have shown to be extremely valuable in extending life

expectancy, by almost a decade for most DMD boys. While these treatments hold short-term benefits, a permanent cure is needed. Furthermore, as treatments are developed a non- invasive assessment such as medical imaging may provide insight into regenerative therapeutic capacity.

1.3   MUSCLE WASTING

In DMD patients muscle strains and tears occur more easily as a result of movement and stretching when the muscle is contracted compared to healthy individuals. Movements requiring eccentric contractions are particularly injurious to DMD patients. Eccentric contractions occur when a muscle lengthens during activation.[22] In these cases, there are no external causes of trauma. As well, muscle damage is heterogeneous; certain muscles are injured more than others are. Muscles used for high-speed activities or rapid acceleration contain a high percentage of type-2 (fast twitch) fibers which are more predisposed to injury. In addition, muscles in which the origin and insertion cross two joints are more at risk for rupture.[23] The rectus femoris, the bicep femoris and the medial head of the gastrocnemius display all these risk factors: they cross two joints and act eccentrically at high speeds. The gastrocnemius in particular has been shown to incur much damage and for this reason is typically a muscle of interest for research studies.[24] Currently, no established solution other than limiting patient movement is effective in reducing muscle wasting. Thus, understanding the genetic and structural components of DMD will provide insight to the disease as a whole.

1.4   GENETIC DEFICIENCY

DMD is an inherited X-linked recessive disease. The DMD gene is located on the

short arm of the human X chromosome. The gene was found to be the largest gene in the

human genome, spanning >2500 kilo base pairs of the X chromosome and occupying

~0.1% of the entire human genome.[25] In 1987, the protein product translated from the

DMD gene was discovered and named dystrophin.[5] It was later discovered that DMD is

caused predominately by deletions in the dystrophin gene that result in a truncated and/or

non-functional dystrophin protein product. It has been shown that dystrophin is a critical

protein in the dystrophin-glycoprotein complex and helps maintain the structural integrity

at the periphery of myofibers. Lack of this protein will result in mechanical and potential

signalling deficiencies seen in DMD patients.

1.5   DYSTROPHIN-GLYCOPROTEIN COMPLEX (DGC)

The DGC is part of the costamere, which helps tether the sarcolemma to

peripheral myofibers of muscle cells (Fig 1.1). As discussed, the cause of many muscular

dystrophies is a defect in the DGC. The DGC consists of a group of membrane proteins

that connects the cytoskeleton of muscle cells to the extracellular matrix. The complex

consists of a number of different proteins, which provide stability between the

extracellular matrix and the actin fibers; a mesh network surrounding the contractile units

within a muscle cell. The DGC plays a crucial role in the maintenance and structural

integrity of the link between the basal lamina and actin fibers.[26] Another function of the

DGC is mechanotransduction which requires proteins such as dystrophin and
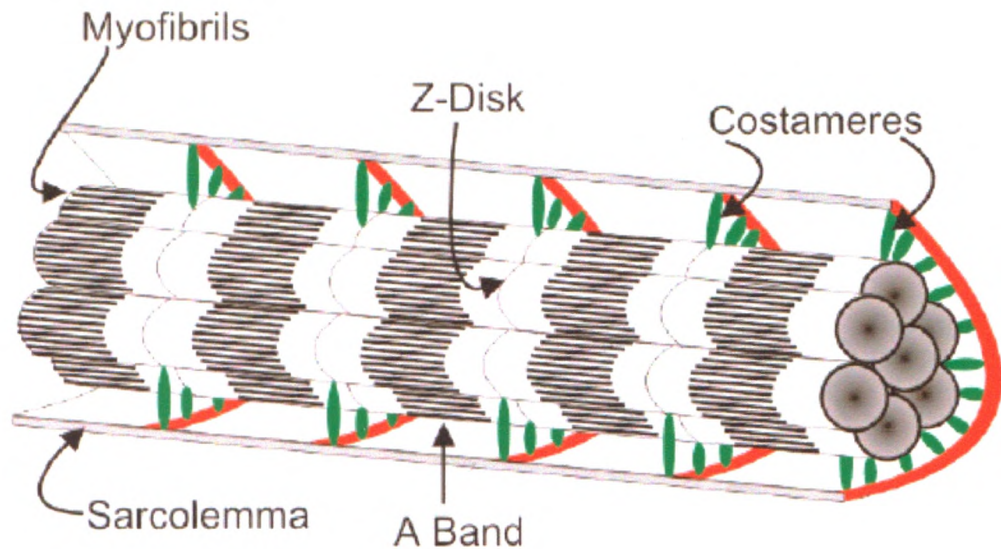
Figure 1.1: Cross-section of myofiber. Image depicts the sarcolemma (cell membrane) which envelops the myofibrils; costameres are present as attachments between the sarcolemma and myofibers.

sarcoglycan-delta.[27] The proteins included within the DGC complex are dystrophin, dystroglycans, sarcoglycans, sarcospan, dystrobrevin, and the syntrophins (Fig 1.2).

1.5.1   Sarcolemma

The sarcolemma is the cell membrane of a myofiber and is an important structural as well as functional component which can be adversely affected from the lack of dystrophin. The sarcolemma acts as a protective barrier which maintains the intracellular environment of a muscle cell. The absence of dystrophin promotes muscle instability by increasing contraction-induced damage to the sarcolemma membrane allowing cytosolic Ca^{+2} levels to increase thereby, initiating a cascade of intracellular events that lead to necrosis.[28,29] Disruption of the membrane will also cause interference in the transmission

Figure 1.2: Diagram of the dystrophin-glycoprotein complex (DGC) and the muscle cell membrane (sarcolemma). Dystrophin is located inside the cell and binds actin fiber at its N-terminus and the syntrophins, sarcoglycans, and dystrobrevin at the C-terminus. Mutations in dystrophin are responsible for DMG / Becker Muscular Dystrophy (DMD/BMD).

of impulse signals, decreasing the ability to synchronize waves of calcium discharge with muscle contractions. Further elevations of Ca^{2+} levels in muscle result from persistently activated calcium leak channels which are incorporated into the membrane during repair.[28,30] Thus, within myocytes with disrupted sarcolemma it has been suggested that continual activation of calcium channels, causes calcium loading resulting in

myonecrosis and tissue calcification.[31] The elevated levels of calcium pose another threat as calcium is also shown to correlate with increased protein degradation.[32] One hypothesis suggests that a rise in cytosolic calcium can cause activation of the proteolytic enzyme, calpain, which may digest contractile proteins, in turn rendering the muscle much weaker.[32]

1.6   DYSTROPHIN AND UTROPHIN

Dystrophin consists of 3,685 amino acids and is primarily expressed in skeletal, cardiac and smooth muscle cells.[33] Dystrophin is a large membrane-associated protein expressed in muscle that is localized to the inner face of the cell membrane.[34,35] Shorter dystrophin isoforms also exist, however they function in non-muscular tissue such as the peripheral nerves, brain, retina and in utero during fetal development.[34] The dystrophin structure can be divided into four domains, each of the four domains except one, the cystein-rich segment, has substantial homology with another known molecule, utrophin.[36]

Utrophin, an autosomal homologue of dystrophin expressed ubiquitously in humans, is another structural protein. The range of tissues where utrophin is expressed is much wider than dystrophin. Utrophin has been demonstrated in normal and mdx mouse brain, stomach, kidney, spleen, liver and lung, and mRNA has been detected in human placenta and adult and foetal skeletal muscle. In human skeletal muscle, utrophin is normally found at the post synaptic membranes of the neuromuscular junction.[37] It is necessary for normal membrane maintenance, and for gathering acetylcholine receptors for efficient activation.[38] As well, utrophin appears to be expressed at higher levels in foetal muscle compared to adult and during mammalian fetal development utrophin is

initially localized to the sarcolemma in place of dystrophin.[39] Interestingly, during the degenerative process high levels of utrophin have also been found around the sarcolemma of regenerating myofibers in adult mdx skeletal muscle.[40-42] Thus, the redundancy in function detected between these two proteins led to the hypothesis that utrophin might be capable, in part, of replacing dystrophin in adult tissue. If so the up-regulation of the utrophin protein may be of important therapeutic strategy in the treatment of DMD.

1.7   MOUSE MODELS USED

Presently, the standard mouse model to study DMD is the mdx (mutated dystrophin on X-chromosome) mouse. These animals are convenient to use because the life span of mice is shorter in comparison to other models such as the golden retriever. As well, the effects of the mutated dystrophin and response to treatment can be studied within a much shorter period of time resulting in large savings in maintenance cost of the mdx mouse model.

The mdx mouse has a point mutation in the dystrophin gene rendering dystrophin non-functional. However, the nature of the progressive muscle-wasting disease presents a much milder form than in humans [37] and the mice often live up to 2 years of age, which is comparable to the life span of wild-type mice. Mdx muscle appears histologically normal in the immediate postnatal period, but an acute phase of muscle necrosis and visible muscle weakness occurs around weaning.[43] At this time, many cellular and biochemical features indicative of muscle degeneration such as elevated serum creatine kinase (CK) levels and accumulation of macrophages become evident. Mdx skeletal muscle then recovers by substantial muscle regeneration, shown by centrally located nuclei in

histology. Up-regulated levels of muscle transcription factors appear to be important components of this successful regeneration. Studies have also shown that mdx mice, lacking the muscle-specific transcription factor MyoD, show a more severe dystrophy due to a deficiency in regenerative capabilities of the muscle.[44]

Compensation for lack of dystrophin by structurally related proteins such as utrophin has been noted in the mdx mouse, leading to a milder phenotype than in humans. At present, the regulation of utrophin is not fully understood. As mentioned there is a substantial body of evidence demonstrating that in mice utrophin is capable of localizing to the sarcolemma where dystrophin typically binds to actin.[45] Additionally, studies on mdx mice in which utrophin over-expression has been induced by transgenic breeding, has shown to relieve murine muscular dystrophy.[46] In contrast the generation of mice which are null mutants of only utrophin, show a very mild phenotype and no outward signs of disease. Lacking only utrophin, has shown to create defects at the neuromuscular junction and a reduction in the number of its functional folds.[47] Suggesting that utrophin does not play a major role in the formation of the clusters at the neuromuscular junction but rather that it may play a role in the development and stabilisation of the folds.[47] Therefore, another mouse model the udx mouse from the breeding of mdx mice with heterozygous utrophin-null mice is also of interest. This model lacks both utrophin and functional dystrophin and displays a severely dystrophic phenotype, premature death, and many cellular characteristics of DMD suggesting that the mild phenotype seen in mdx mice may be due to the compensating effect of utrophin. Therefore, both of these models remain of research interest and each provides differential insight in terms of severity and progressiveness for the characterization of murine DMD.

1.8   PRE-CLINICAL TREATMENTS

There are currently several different pre-clinical approaches, which have provided hope towards a cure for DMD. In 2003, an Australian group attempted a gene-based therapy. Wokke et al. proposed a therapy based on the principle of exon skipping. Exons are units of genetic information within a gene, each exon codes for specific portion of a complete gene. By skipping mutated exons, the translated protein while truncated, may remain functional, producing a milder phenotype if not a cure for the disease. However due to the length of the dystrophin gene this approach was proven to be difficult. [48,49] In 1996, another study, utilizing virally-directed transgenic dystrophin synthesis, was attempted.[50] Kapsa et al. attempted to express the dystrophin protein in muscle groups. However, they found that long term maintenance could not be achieved due to immune rejection and virulence of the vectors.[50] Other groups attempted transplantation of myoblasts into muscle. Myoblasts are muscle precursor cells that can be isolated from muscle tissue and amplified by proliferation in tissue culture. It was intended that the transplanted cells then divide and fuse to form new muscle fibers. However, several limitations to this approach quickly emerge which include immune rejection, limited spread and proliferation of transplanted cells, lack of fusion into fibers due to fibrosis, and poor cell survival rates.[51] Another approach as mentioned earlier is up-regulation of utrophin. Utrophin is an analog of dystrophin and is shown to be up-regulated in dystrophin deficient mdx mice to produce a milder disease phenotype. Research has been conducted to identify if utrophin can be up-regulated and relocated in the absences of functional dystrophin.[37] Accordingly, if expression of utrophin is sufficiently elevated, it may maintain the DGC and thus alleviate muscle damage.[37,38] The expression of a utrophin minigene under the control of a human *a*-skeletal actin promoter in mdx mice

has been shown to restore some function of the DGC to the sarcolemma and to result in mice with slightly improved muscle pathology.[52] If utrophin were to be up-regulated in human DMD patients, similar results to those seen in the mdx mice might be expected.[53] Further studies are needed to determine if the "utrophin substitution" for dystrophin is effective in human DMD patients.

While each of the discussed approaches holds promise for a cure of DMD, they lack non-invasive methods of treatment assessment. While histology is the gold standard to assess treatment efficacy, non-invasive imaging biomarkers will provide quantitative functional information to complement the histological results.

1.9 PHYSIOLOGICAL CHANGES

While structural and degenerative changes occur in skeletal muscle, other functional processes may also be affected by the absence of dystrophin. These will be examined in the following sections.

1.9.1 Smooth Muscle

Smooth muscle is responsible for the contractility of hollow organs, such as blood vessels. Dystrophin is expressed in both vascular smooth muscle cells and endothelial cells which are normally subjected to axial/circumferential shear stresses to accommodate changes in blood flow and blood volume.[54] Degenerative effects on smooth muscle due to non-functional dystrophin may in turn alter vasoreactivity. Early studies of DMD suggest a theory of disease progression that involve defects in the microcirculation due to the loss of dystrophin causing irregularities in capillary structure and hindering regular

function. For example, abnormalities were apparent in capillary beds of the biceps brachii of very young DMD patients in the preclinical stages of the disease. Electron microscopy revealed swollen endothelial cells in ~30% of small vessels, increased capillary wall and endothelial cell areas, and thicker basement membrane around the vessels.[55,56] Furthermore, sympathetic neurovascular control is abnormal in dystrophin-deficient muscle. This defective regulation is observed during exercise, when sympathetic vasoconstriction normally is blunted in the active muscles by locally produced dilator substances such as nitric oxide (NO).[54] Thus, due to mechanical insufficiencies in smooth muscles, an aberrant myogenic response may in turn limit the body's ability to regulate flow and fulfill metabolic demands when required.

1.9.2 Inflammatory Response

Inflammation is a complex response due to some form of irritant, insult or injury. In DMD patients, muscle inflammation is a characteristic feature due to instability within the DGC.[57] The chronic myositis seen in DMD patients, in turn induces the release of many cytokines that act as signalling proteins and vasomediators to both nearby or distant cells throughout the body.[58] In a chronic state macrophages have shown to have a life span of months to years. Chronic inflammation and fibrosis in dystrophic muscle is of research interest because inflammation can potentially alter the normal hemodynamic responses in affected individuals.[59, 60] Wehling et al. suggested that the major damage in DMD might actually be secondary to the loss of functioning dystrophin. This group has suggested that the destruction of muscle tissue may primarily occur by a patient's own immune response.[61] The destruction of muscle by macrophage leads to weakened

muscles and fibrosis which accumulates and act as structural filler, decreasing muscle strength and functionality.[57]

It is critical to determine the natural course of inflammation occurring in DMD patients, from such knowledge we may better time interventions to allow the body to work with its immune response instead of against it.

1.9.3   Nitric Oxide Synthase

Three forms of nitric oxide synthase (NOS) exists, however in muscle the most prominent form is neuronal NOS (nNOS).[62] In DMD, due to the lack of functional dystrophin, this synthase is mislocalized from the membrane to the intracellular compartment, reducing its efficiency.[66] Nitric oxide (NO), a product of the nNOS in skeletal muscle, functions to modulate vascular tone, aids in the immune response, assists with the release of calcium modulation or partial inhibition of muscle contraction, and contributes to muscle growth.[63-65] Due to its ability to form reactive oxygen species, NO is also capable of causing necrosis or toxicity in tissue at high concentrations.[67] Complete removal of NO production in mdx mice (nNOS-null mdx double mutant mice) has shown to not improve dystrophy.[68] However, it was later demonstrated that over-expression of nNOS in mdx mice significantly reduced muscular dystrophy.[69] Thus, introduction of a transgene to produce normal/above normal levels of NOS in the muscles reduced the concentrations of macrophages in the muscles, preventing muscle membrane injury in the mdx mouse.[69] Suggesting that the degeneration of muscle seen in DMD is not solely caused by changes in nNOS distribution,[70] yet changes in these distributions may still affect the regulation of hemodynamics.

Therefore, it is important to be able to quantify metabolic, hemodynamic and structural changes in models of DMD. Without a thorough understanding of how and when such compensatory responses occur, it will be difficult to assess disease progression and potential therapies in patients with DMD. The importance of a non-invasive imaging method to assess disease progression cannot be overemphasized.

1.10 MEDICAL IMAGING IN DUCHENNE MUSCULAR DYSTROPHY

Imaging has the potential to provide crucial information on the progression and may assist in the evaluation of newer treatments for DMD. Imaging is used to non-invasively diagnose many health problems from bone fractures to brain tumours. Currently, clinical evaluations of DMD do not utilize medical imaging for disease prognosis or evaluation of disease progression. However, preclinical functional and anatomical imaging has grown as a new approach in understanding disease progression. Modalities such as Magnetic Resonance Imaging (MRI) have been used to detect change in muscle architecture,[71] inflammation,[72] or differences in muscle permeability [73] in mdx mice. As well Single Photon Emission Computed Tomography (SPECT) has been used to evaluate changes in myocardial damage,[74] identify perfusion defects caused by fibrosis and fat infiltration,[75] and measure differences in left ventricular ejection fraction in DMD.[76] However among the many modalities available Computed Tomography (CT), positron emission tomography (PET) and Ultrasound (US) were the preferred methods for the studies conducted in this thesis. Advances in dynamic contrast-enhanced computed tomography (DCE-CT), PET, and high frequency ultrasound (HFU) imaging, have provided researchers and clinicians with high-resolution of anatomical and

functional images of the human body. Each of these imaging modalities provides complimentary information such as hemodynamics, metabolism and structural changes in living subjects. Thus, there is good rationale to use a combination of these different imaging modalities to increase diagnostic sensitivity and specificity in monitoring progression and treatment response of DMD. This study is the first to use DCE-CT, PET and HFU longitudinally to non-invasively assess functional and anatomical changes in skeletal muscle of two murine models of DMD.

1.10.1 Dynamic Contrast Enhanced Computed Tomography (DCE-CT)

With the advancements in fast, multi-slice CT's based on slip-ring technology Dynamic Contrast Enhanced CT (DCE-CT) has gained much acceptance. Benefits of CT include availability, speed of scans, and ability to image a combination of soft tissue, bone, and blood vessels. However, drawbacks include cost and radiation dose.

Previous studies have utilized CT as a prognostic indicator in the development of scoliosis.[78] Further anatomical changes in DMD such as muscle atrophy,[79] accumulation of fat and muscle fibre loss have also successfully been assessed using CT.[80,81] This thesis attempts to quantitate functional hemodynamic changes in dystrophic muscle using DCE-CT. This was accomplished on a preclinical scanner suited for small animals, the eXplore Ultra by General Electric Health Care (GEHC) with a spatial resolution of 175 μm (in-plane) and 900 μm thick slices. Imaging was focused on the hind limbs of the animals in order to assess changes in skeletal muscle perfusion over the length of the study.

In a DCE-CT study, an x-ray iodinate contrast agent is injected into the blood stream via a peripheral vein and the arterial concentration Ca(t), and tissue concentration Q(t), of x-ray contrast is measured using a CT scanner (Fig 1.3b). The principle of this technique relies on the assumptions that the tracer is uniformly mixed within the ventricle and that enhancement in the region is proportional to the tracer concentration. The acquired data together with suitable tracer kinetics modeling permits derivation of heamodynamic information including blood flow (perfusion) and blood volume about the tissue. Upon completion, the image series can be transferred to a workstation for processing to calculate quantitative blood flow (BF) and blood volume (BV) parametric maps.

Parametric maps are calculated on a GE workstation (GE Healthcare) using proprietary software (CT Perfusion, GE Health). The algorithm used for CTP is based on the Johnson Wilson model, a distributed compartmental model with bidirectional flow. Two sets of data in the raw dataset are created; the arterial and the tissue time enhancement curve. Enhancement is the increase in attenuation of x-rays, which increases due to the presence of a contrast agent and is measured in CT numbers. The arterial and tissue time enhancement curves are then deconvolved to determine the blood flow scaled impulse residue function (IRF) (Fig 1.3a). The area under the blood flow scaled IRF corresponds to the blood volume and the height of the blood flow scaled IRF provides blood flow. Using the values obtained for each voxel in the image, maps are produced which display the calculated values according to a colour scale, creating a 2D functional map. The generated functional maps in turn, provide the researcher with the ability to quantify changes in tissue blood flow or volume in a region of interest.
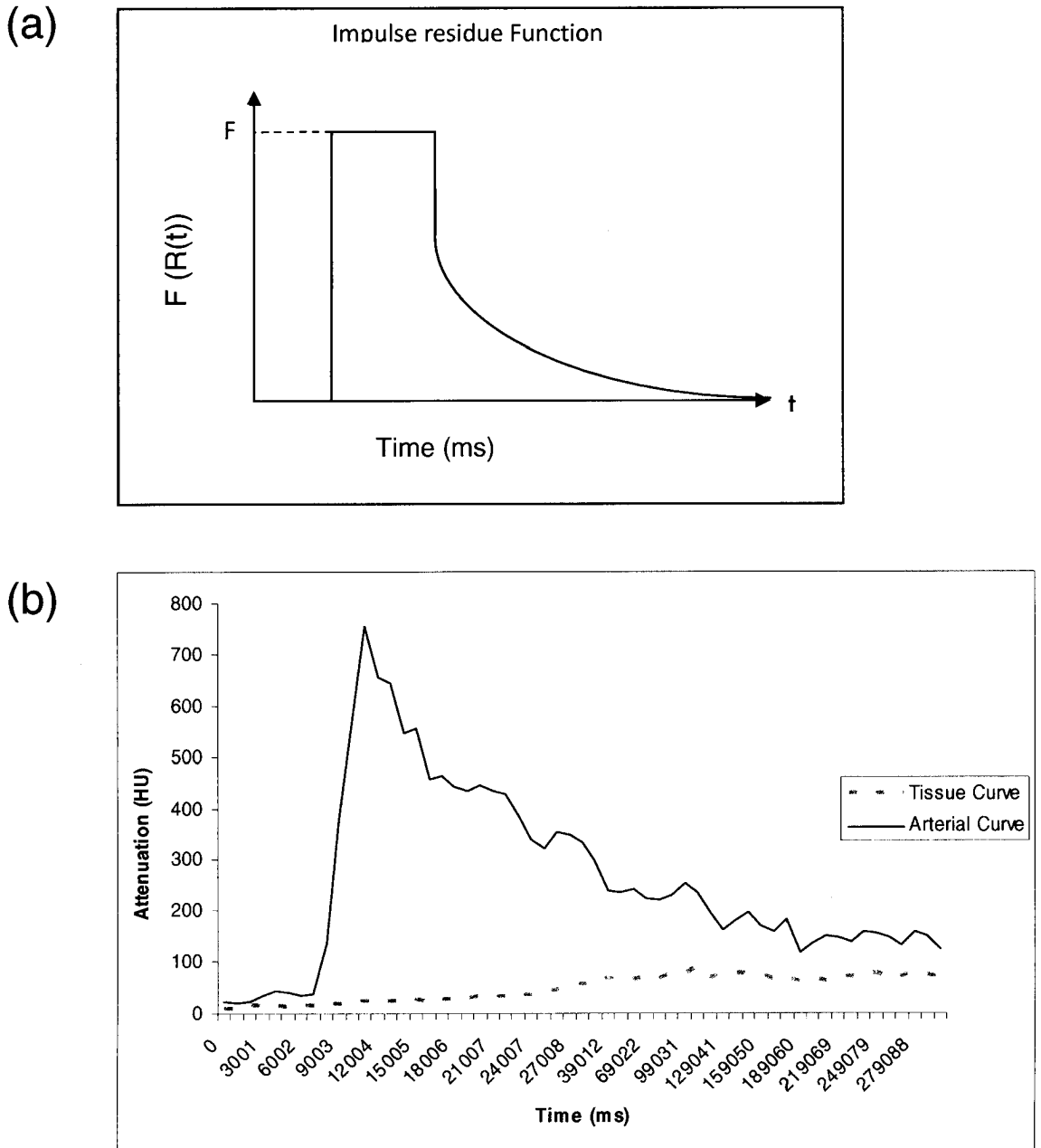
Figure 1.3: (a) Example of an ideal blood flow scaled impulse residue function (IRF) (F = blood flow; R(t) = impulse residue function), obtained from the deconvolution of the arterial input function (AIF) and tissue time-density curve shown in (b).

DEC-CT holds the potential to provide crucial functional information regarding hemodynamic changes in DMD. This in turn will provide a better understanding of when degenerative processes occur and will provide insight for therapies in patients with DMD.

1.10.2 Positron Emission Tomography (PET)

The concept of PET was first introduced in the 1950's.[82] PET is a valuable clinical and research tool in disease diagnosis and prognosis. Benefits of PET include, low radiation dose and the ability to trace biological pathways in living subjects. Limitations of PET include cost, short half-lives of radionuclide, and poor spatial resolution relative to MRI or CT. Previously, PET has been used to detect differences in cardiac metabolism between wild type and dystrophic mice. These studies have shown lower uptake of F-18-flourodeoxyglucose (FDG), a glucose analog, in dystrophic cardiac muscle.[83] As well myocardial perfusion studies in humans, have detected defects in the inferior, anterior, and apical myocardial walls of Becker patients.[84] Furthermore, studies of the left ventricle in muscular dystrophy patients have revealed decreased metabolism, and reductions in regional blood flow.[85] A reduction in brain metabolism was also demonstrated in regions typically rich in dystrophin production in human DMD patients.[86] This thesis attempts to quantitate metabolic changes in dystrophic muscle using PET. For these studies a small animal preclinical PET scanner was used, the eXplore Vista (GE Healthcare). This scanner has the capability of producing a spatial resolution of 1.5 mm radial, 1.6 mm tangential, 1.7 mm axial, and a 3.9-mm^3 volume.

PET targets specific biochemical processes in organs of interest over time and using this calculates functional parameters. PET requires the injection of very small

amounts of radioactive material (tracers) and detection of gamma rays from the decay of the tracers to localize their position. All PET compounds are radio-labelled with positron-emitting radionuclides. The most common PET tracer is F-18-labelled fluorodeoxyglucose, 18F-FDG, a glucose analog, which can be correlated with glucose uptake and metabolism. As the radionuclide decays positrons are emitted, the positrons travel a short distance and annihilate with an electron resulting in two 511 keV photons traveling in opposite directions. The detection of photons localizes the positron emitting radionuclide to be somewhere along the line defined by the two detectors called the line of response. PET detects the photons with scintillation crystals which convert the detection into visible light. The light is detected by photomultiplier tubes, which in turn convert and amplifies the photons to electrical signal. These signals are then processed for coincidence. Coincidence processing determines if two electrical signals originate from the same source. If two electrical signals are detected in opposing detectors within a 12 nanosecond time period they are considered to be a coincident event. A computer receives and processes all the coincident events to determine the projection of radioisotope concentration in different directions. Once a complete set of projections from all angles (360°) around the object is acquired, a filtered back projection algorithm is applied to reconstruct images of the distribution of radioisotope concentration within a living subject. This algorithm is advantageous because it requires low computing resources however; a disadvantage is that with regions of high uptake such as the bladder streaks appear. In a FDG PET study, the end result is an image in which the pixel values are proportional to the accumulation of FDG, which is an indicator of glucose metabolic rate.

PET holds the promise to be a powerful modality for studying DMD, as it is capable of providing absolute quantitation of metabolic processes. If metabolic changes can be detected in dystrophic muscle longitudinally, PET will provide a non-invasive assessment of the progression of muscle degeneration as well as monitoring of future therapies.

1.10.3 High Frequency Ultrasound (HFU)

Ultrasound (US) has been used as a quick and effective method to non-invasively image muscles and internal organs, their size, structures and possible pathologies or lesions. Benefits to using ultrasound are that patients are not exposed to ionizing radiation, short scan times and low operational costs. Drawbacks however include inter-operator variability, which depends on levels of experience. Ultrasound has been used to assess architectural changes in muscle such as fatty infiltration, muscle tears, and atrophy.[87] Furthermore, US has been used to measure muscle thickness, ratio of muscle thickness to subcutaneous fat thickness, and echo intensity in muscle.[88] US imaging in this thesis was used to assess degenerative changes in dystrophic skeletal muscle. Imaging was accomplished using the Vevo 770 High Frequency Ultrasound (HFU) scanner. Three-dimensional images were reconstructed and visualized using Visual Sonics software.[89] The systems image resolution capabilities are 40 μm axial and 80 μm lateral at a maximum focal depth of 6mm.

US produces images by using a pulse-echo approach with a brightness mode (B-mode) display. This involves transmitting short pulses of ultrasound into the body, which are reflected from structures and detected upon return by the transducer. While typical

clinical ultrasounds operate at 10-20 MHz, high frequency ultrasound (HFU) scanners as the Vevo 770 operate at 40 MHz. The choice of frequency is a trade-off between spatial resolution of the image and imaging depth: higher frequencies have better resolution but have very limited depth of penetration into the body compared to lower frequencies.

Injured muscle can cause profound changes in an ultrasound image, including increased echogenicity and homogeneity within muscle. The increased echogenicity of muscle reflects an increased number of acoustic interfaces related to fat accumulation, fibrosis, and inflammation.[90] In addition, the injury/disease process blurs the distinction between the fibroadipose septa of myofibers and muscle fascicles, making the image more homogeneously echogenic.[90] Thus, ultrasound has the potential to be used as a diagnostic tool to characterize changes in dystrophic muscle over time.

1.11 RESEARCH GOALS

The goals of this project were to follow the progression of disease in two murine models of muscular dystrophy (mdx and udx mice) over a 16-week period against wild-type mice as control. The three goals were:

(1) To compare hemodynamic (blood flow and blood volume) changes in skeletal muscle measured by DCE-CT;

(2) To compare the metabolic changes in skeletal muscle using an FDG-PET study;

(3) To compare architectural/morphological changes in skeletal muscle using High Frequency Ultrasound.

1.12   THESIS OUTLINE

Chapter 2 presents a study investigating the progression of disease in mdx and udx mice in comparison to wild type mice using DCE-CT and PET. In addition, these results were correlated with histology to aid their interpretations. This chapter is based on the paper entitled "Functional Imaging of Disease Progression in Murine Models of Duchenne Muscular Dystrophy" which was submitted for publication to Molecular Imaging. My contributions towards this study were performing animal experiments, data collection and analysis, statistical analysis, and writing/editing revisions of manuscript.

Chapter 3 presents a study investigating muscle injury in mdx and udx mice using high frequency ultrasound (HFU). We proposed a new grading system to assess muscle injury using three parameters (1) number of lesions, (2) size of lesions, (3) muscle disorganization. Skeletal muscle of the hind limb, specifically the gastrocnemius was imaged over a 16 week period and graded for damage in mdx (exercised and non-exercised), udx (non-exercised) and wt (exercised) mice. These findings were then compared against histology as a validation of HFU ability to correctly assess muscle injury. This chapter is based on a paper entitled "High frequency ultrasound as a non-invasive tool to assess disease progression in murine models of Duchenne Muscular Dystrophy" which was submitted for publication to the Journal of Ultrasound in Medicine. My contributions towards this study were performing animal experiments, data collection and analysis, statistical analysis, and writing/editing revisions of manuscript.

Chapter 4 provides a summary of findings from both chapters 2 and 3, followed by concluding statements and suggestions of future work on moving towards therapeutic options for DMD.

1.13 REFERENCES

1. Dalkilic I KLM. Muscular dystrophies: Genes to pathogenesis. *Current Opinion in Molecular Genetics and Development* 2003;13:231-238.

2. Reitter B, Goebel HH. Dystrophinopathies. *Semin Pediatr Neurol* 1996;3:99-109.

3. Monaco AP, Bertelson CJ, Liechti-Gallati S, Moser H, Kunkel LM. An explanation for the phenotypic differences between patients bearing partial deletions of the DMD locus. *Genomics* 1988;2:90-5.

4. Ahn AH, Kunkel LM. The structural and functional diversity of dystrophin. *Nat Genet* 1993;3:283-91.

5. Hoffman EP, Brown RH, Jr., Kunkel LM. Dystrophin: the protein product of the Duchenne muscular dystrophy locus. *Cell* 1987;51:919-28.

6. Duchenne G. Research on the paralysis seen in muscle with pseudohypertrophy. *Arch Gen Med* 1868;11:5.

7. Tyler KL. Origins and early descriptions of "Duchenne muscular dystrophy". *Muscle Nerve* 2003;28:402-22.

8. Bideau Y. The Duchenne muscular dystrophy child: care of wheelchair-dependent patient Death prevention. *Muscle Nerve* 1986;9:86.

9. Dubowitz V. Myopathic Changes in a Muscular Dystrophy Carrier. *J Neurol Neurosurg Psychiatry* 1983;26:322-5.

10. Worden DK, Vignos PJ, Jr. Intellectual function in childhood progressive muscular dystrophy. *Pediatrics* 1962;29:968-77.

11. Ptacek L, Johnson, KJ, Griggs, RC. Mechanisms of Disease: Genetics and Physiology of the Myotonic Muscle Disorders. *NEJM* 1993:482-489.

12. Gowers WR. Clinical lecture on pseudo-hypertrophic muscular paralysis. *lANCET* 1879;2:1-2.

13. Smith AD, Koreska J, Moseley CF. Progression of scoliosis in Duchenne muscular dystrophy. *J Bone Joint Surg Am* 1989;71:1066-74.

14. Mendell J. Griggs RC. Ptacek L J. Harrison's Textbook of Internal Medicine - Diseases of Muscle New York: McGraw-Hill, 1998:2473-2483.

15. Shapiro F, Specht L. The diagnosis and orthopaedic treatment of inherited muscular diseases of childhood. *J Bone Joint Surg Am* 1993;75:439-54.

16.   Ebashi S, Toyokura,Y. Momoi,H. Sugita,H. High creatine phosphokinase activity of sera of progressive muscular dystrophy. *J Biochem* 1959;46:103.

17.   Hess JW, Macdonald RP, Frederick RJ, Jones RN, Neely J, Gross D. Serum Creatine Phosphokinase (Cpk) Activity in Disorders of Heart and Skeletal Muscle. *Ann Intern Med* 1964;61:1015-28.

18.   McDonald CM. Limb contractures in progressive neuromuscular disease and the role of stretching, orthotics, and surgery. *Phys Med Rehabil Clin N Am* 1998;9:187-211.

19.   Bach JR, McKeon J. Orthopedic surgery and rehabilitation for the prolongation of brace-free ambulation of patients with Duchenne muscular dystrophy. *Am J Phys Med Rehabil* 1991;70:323-31.

20.   Baydur A CI, Prentice W Guidelines for assisted ventilation in Duchenne muscular dystrophy. *Am Rev Respir Dis* 1985;131:A268.

21.   Curran FJ. Night ventilation by body respirators for patients in chronic respiratory failure due to late stage Duchenne muscular dystrophy. *Arch Phys Med Rehabil* 1981;62:270-4.

22.   Ciullo JV, Zarins B. Biomechanics of the musculotendinous unit: relation to athletic performance and injury. *Clin Sports Med* 1983;2:71-86.

23.   Noonan TJ, Garrett WE, Jr. Muscle strain injury: diagnosis and treatment. *J Am Acad Orthop Surg* 1999;7:262-9.

24.   Brussee V, Tardif F, Tremblay JP. Muscle fibers of mdx mice are more vulnerable to exercise than those of normal mice. *Neuromuscul Disord* 1997;7:487-92.

25.   Ozawa E, Noguchi S, Mizuno Y, Hagiwara Y, Yoshida M. From dystrophinopathy to sarcoglycanopathy: evolution of a concept of muscular dystrophy. *Muscle Nerve* 1998;21:421-38.

26.   Pasternak C, Wong S, Elson EL. Mechanical function of dystrophin in muscle cells. *J Cell Biol* 1995;128:355-61.

27.   Hack AA, Lam MY, Cordier L, Shoturma DI, Ly CT, Hadhazy MA, Hadhazy MR, Sweeney HL, McNally EM. Differential requirement for individual sarcoglycans and dystrophin in the assembly and function of the dystrophin-glycoprotein complex. *J Cell Sci* 2000;113 (Pt 14):2535-44.

28. Alderton JM, Steinhardt RA. Calcium influx through calcium leak channels is responsible for the elevated levels of calcium-dependent proteolysis in dystrophic myotubes. *J Biol Chem* 2000;275:9452-60.

29. Ruegg UT, Gillis JM. Calcium homeostasis in dystrophic muscle. *Trends Pharmacol Sci* 1999;20:351-2.

30. Petrof BJ. Molecular pathophysiology of myofiber injury in deficiencies of the dystrophin-glycoprotein complex. *Am J Phys Med Rehabil* 2002;81:S162-74.

31. Elsherif L, Huang MS, Shai SY, Yang Y, Li RY, Chun J, Mekany MA, Chu AL, Kaufman SJ, Ross RS. Combined deficiency of dystrophin and beta1 integrin in the cardiac myocyte causes myocardial dysfunction, fibrosis and calcification. *Circ Res* 2008;102:1109-17.

32. Hussain T, Kumar DV, Sundaram C, Mohandas S, Anandaraj MP. Quantitative ELISA for platelet m-calpain: a phenotypic index for detection of carriers of Duchenne muscular dystrophy. *Clin Chim Acta* 1998;269:13-20.

33. Koenig M, Monaco AP, Kunkel LM. The complete sequence of dystrophin predicts a rod-shaped cytoskeletal protein. *Cell* 1988;53:219-28.

34. Blake DJ, Weir A, Newey SE, Davies KE. Function and genetics of dystrophin and dystrophin-related proteins in muscle. *Physiol Rev* 2002;82:291-329.

35. Deconinck AE, Rafael JA, Skinner JA, Brown SC, Potter AC, Metzinger L, Watt DJ, Dickson JG, Tinsley JM, Davies KE. Utrophin-dystrophin-deficient mice as a model for Duchenne muscular dystrophy. *Cell* 1997;90:717-27.

36. Matsumura K, Ervasti JM, Ohlendieck K, Kahl SD, Campbell KP. Association of dystrophin-related protein with dystrophin-associated proteins in mdx mouse muscle. *Nature* 1992;360:588-91.

37. Love DR, Hill DF, Dickson G, Spurr NK, Byth BC, Marsden RF, Walsh FS, Edwards YH, Davies KE. An autosomal transcript in skeletal muscle with homology to dystrophin. *Nature* 1989;339:55-8.

38. Tinsley JM, Davies KE. Utrophin: a potential replacement for dystrophin? *Neuromuscul Disord* 1993;3:537-9.

39. Bewick GS, Nicholson LV, Young C, O'Donnell E, Slater CR. Different distributions of dystrophin and related proteins at nerve-muscle junctions. *Neuroreport* 1992;3:857-60.

40. Sewry CA, Matsumura K, Campbell KP, Dubowitz V. Expression of dystrophin-associated glycoproteins and utrophin in carriers of Duchenne muscular dystrophy. *Neuromuscul Disord* 1994;4:401-9.

41. Karpati G, Acsadi G. The potential for gene therapy in Duchenne muscular dystrophy and other genetic muscle diseases. *Muscle Nerve* 1993;16:1141-53.

42. Helliwell TR, Man NT, Morris GE, Davies KE. The dystrophin-related protein, utrophin, is expressed on the sarcolemma of regenerating human skeletal muscle fibres in dystrophies and inflammatory myopathies. *Neuromuscul Disord* 1992;2:177-84.

43. Cullen MJ, Jaros E. Ultrastructure of the skeletal muscle in the X chromosome-linked dystrophic (mdx) mouse. Comparison with Duchenne muscular dystrophy. *Acta Neuropathol* 1988;77:69-81.

44. Megeney LA, Kablar B, Garrett K, Anderson JE, Rudnicki MA. MyoD is required for myogenic stem cell function in adult skeletal muscle. *Genes Dev* 1996;10:1173-83.

45. Winder SJ, Hemmings L, Maciver SK, Bolton SJ, Tinsley JM, Davies KE, Critchley DR, Kendrick-Jones J. Utrophin actin binding domain: analysis of actin binding and cellular targeting. *J Cell Sci* 1995;108 (Pt 1):63-71.

46. Rafael JA, Brown SC. Dystrophin and utrophin: genetic analyses of their role in skeletal muscle. *Microsc Res Tech* 2000;48:155-66.

47. Rafael JA, Townsend ER, Squire SE, Potter AC, Chamberlain JS, Davies KE. Dystrophin and utrophin influence fiber type composition and post-synaptic membrane structure. *Hum Mol Genet* 2000;9:1357-67.

48. Mann CJ, Honeyman K, Cheng AJ, Ly T, Lloyd F, Fletcher S, Morgan JE, Partridge TA, Wilton SD. Antisense-induced exon skipping and synthesis of dystrophin in the mdx mouse. *Proc Natl Acad Sci U S A* 2001;98:42-7.

49. Wokke J. Genes, Trials, and care: the dynamics of neuromeuscular disease. . *The Lancet Neurology* 2004;3:16.

50. Kapsa R, Kornberg AJ, Byrne E. Novel therapies for Duchenne muscular dystrophy. *Lancet Neurol* 2003;2:299-310.

51. Huard J, Cao B, Qu-Petersen Z. Muscle-derived stem cells: potential for muscle regeneration. *Birth Defects Res C Embryo Today* 2003;69:230-7.

52. Tinsley JM, Potter AC, Phelps SR, Fisher R, Trickett JI, Davies KE. Amelioration of the dystrophic phenotype of mdx mice using a truncated utrophin transgene. *Nature* 1996;384:349-53.

53. Jasmin BJ, Angus LM, Belanger G, Chakkalakal JV, Gramolini AO, Lunde JA, Stocksley MA, Thompson J. Multiple regulatory events controlling the expression and localization of utrophin in skeletal muscle fibers: insights into a therapeutic strategy for Duchenne muscular dystrophy. *J Physiol Paris* 2002;96:31-42.

54. Loufrani L, Matrougui K, Gorny D, Duriez M, Blanc I, Levy BI, Henrion D. Flow (shear stress)-induced endothelium-dependent dilation is altered in mice lacking the gene encoding for dystrophin. *Circulation* 2001;103:864-70.

55. Miike T, Sugino S, Ohtani Y, Taku K, Yoshioka K. Vascular endothelial cell injury and platelet embolism in Duchenne muscular dystrophy at the preclinical stage. *J Neurol Sci* 1987;82:67-80.

56. Mechler F, Mastaglia FL, Haggith J, Gardner-Medwin D. Adrenergic receptor responses of vascular smooth muscle in Becker dystrophy. A muscle blood flow study using the 133Xe clearance method. *J Neurol Sci* 1980;46:291-302.

57. Janeway C, Travers, P. Immunobiology -the immune system in health and disease. . Garland Publishing, Inc., 2001.

58. Scriver CR, Beaudet, A. L., Sly, W. S., Valle, D, Childs, B., Kinzler, K. W., and Vogelstein, B. The Metabolic and Molecular Bases of Inherited Disease McGraw-Hill, New-York, 2001:7012.

59. Nielsen S, Pedersen BK. Skeletal muscle as an immunogenic organ. *Curr Opin Pharmacol* 2008;8:346-51.

60. Farini A, Meregalli M, Belicchi M, Battistelli M, Parolini D, D'Antona G, Gavina M, Ottoboni L, Constantin G, Bottinelli R, Torrente Y. T and B lymphocyte depletion has a marked effect on the fibrosis of dystrophic skeletal muscles in the scid/mdx mouse. *J Pathol* 2007;213:229-38.

61. Wehling-Henricks M, Sokolow S, Lee JJ, Myung KH, Villalta SA, Tidball JG. Major basic protein-1 promotes fibrosis of dystrophic muscle and attenuates the cellular immune response in muscular dystrophy. *Hum Mol Genet* 2008;17:2280-92.

62. Kaminski HJ, Andrade FH. Nitric oxide: biologic effects on muscle and role in muscle diseases. *Neuromuscul Disord* 2001;11:517-24.

63. Reid MB. Nitric oxide, reactive oxygen species, and skeletal muscle contraction. *Med Sci Sports Exerc* 2001;33:371-6.

64.   Stamler JS, Meissner G. Physiology of nitric oxide in skeletal muscle. *Physiol Rev* 2001;81:209-237.

65.   Tidball JG, Spencer MJ, Wehling M, Lavergne E. Nitric-oxide synthase is a mechanical signal transducer that modulates talin and vinculin expression. *J Biol Chem* 1999;274:33155-60.

66.   Brenman JE, Chao DS, Xia H, Aldape K, Bredt DS. Nitric oxide synthase complexed with dystrophin and absent from skeletal muscle sarcolemma in Duchenne muscular dystrophy. *Cell* 1995;82:743-52.

67.   Thomas GD, Shaul PW, Yuhanna IS, Froehner SC, Adams ME. Vasomodulation by skeletal muscle-derived nitric oxide requires alpha-syntrophin-mediated sarcolemmal localization of neuronal Nitric oxide synthase. *Circ Res* 2003;92:554-60.

68.   Chao DS, Silvagno F, Bredt DS. Muscular dystrophy in mdx mice despite lack of neuronal nitric oxide synthase. *J Neurochem* 1998;71:784-9.

69.   Wehling M, Spencer MJ, Tidball JG. A nitric oxide synthase transgene ameliorates muscular dystrophy in mdx mice. *J Cell Biol* 2001;155:123-31.

70.   Kameya S, Miyagoe Y, Nonaka I, Ikemoto T, Endo M, Hanaoka K, Nabeshima Y, Takeda S. alpha1-syntrophin gene disruption results in the absence of neuronal-type nitric-oxide synthase at the sarcolemma but does not induce muscle degeneration. *J Biol Chem* 1999;274:2193-200.

71.   McIntosh LM, Baker RE, Anderson JE. Magnetic resonance imaging of regenerating and dystrophic mouse muscle. *Biochem Cell Biol* 1998;76:532-41.

72.   Mercuri E, Pichiecchio A, Allsop J, Messina S, Pane M, Muntoni F. Muscle MRI in inherited neuromuscular disorders: past, present, and future. *J Magn Reson Imaging* 2007;25:433-40.

73.   Straub V, Donahue KM, Allamand V, Davisson RL, Kim YR, Campbell KP. Contrast agent-enhanced magnetic resonance imaging of skeletal muscle damage in animal models of muscular dystrophy. *Magn Reson Med* 2000;44:655-9.

74.   Tamura T, Shibuya N, Hashiba K, Oku Y, Mori H, Yano K. Evaluation of myocardial damage in Duchenne's muscular dystrophy with thallium-201 myocardial SPECT. *Jpn Heart J* 1993;34:51-61.

75.   Nishimura T, Yanagisawa A, Sakata H, Sakata K, Shimoyama K, Ishihara T, Yoshino H, Ishikawa K. Thallium-201 single photon emission computed tomography (SPECT) in patients with duchenne's progressive muscular dystrophy: a histopathologic correlation study. *Jpn Circ J* 2001;65:99-105.

76.   Mansi L, Pace L, Politano L, Rambaldi PF, Di Gregorio F, Raia P, Petretta VR, Nigro G. Left ventricular function and perfusion in Becker's muscular dystrophy. *J Nucl Med* 1997;38:563-7.

77.   Axel L. Cerebral blood flow determination by rapid-sequence computed tomography: theoretical analysis. *Radiology* 1980;137:679-86.

78.   Stern LM, Clark BE. Investigation of scoliosis in Duchenne dystrophy using computerized tomography. *Muscle Nerve* 1988;11:775-83.

79.   Miyashita I, Yamamoto H, Koga H, Kani K, Mori K. [Computed tomography of skeletal muscles in myotonic muscular dystrophy]. *Rinsho Shinkeigaku* 1990;30:24-8.

80.   Liu M, Chino N, Ishihara T. Muscle damage progression in Duchenne muscular dystrophy evaluated by a new quantitative computed tomography method. *Arch Phys Med Rehabil* 1993;74:507-14.

81.   Saitoh H. [CT findings of muscular dystrophy: limb girdle type (LG), myotonic type (MYD) and Duchenne type (DMD)]. *Nippon Igaku Hoshasen Gakkai Zasshi* 1991;51:790-8.

82.   Ter-Pogossian MM, Phelps ME, Hoffman EJ, Mullani NA. A positron-emission transaxial tomograph for nuclear imaging (PETT). *Radiology* 1975;114:89-98.

83.   Quinlivan RM, Lewis P, Marsden P, Dundas R, Robb SA, Baker E, Maisey M. Cardiac function, metabolism and perfusion in Duchenne and Becker muscular dystrophy. *Neuromuscul Disord* 1996;6:237-46.

84.   Quinlivan R, Ball J, Dunckley M, Thomas DJ, Flinter F, Morgan-Hughes J. Becker muscular dystrophy presenting with complete heart block in the sixth decade. *J Neurol* 1995;242:398-400.

85.   Perloff JK, Henze E, Schelbert HR. Alterations in regional myocardial metabolism, perfusion, and wall motion in Duchenne muscular dystrophy studied by radionuclide imaging. *Circulation* 1984;69:33-42.

86.   Lee JS, Pfund Z, Juhasz C, Behen ME, Muzik O, Chugani DC, Nigro MA, Chugani HT. Altered regional brain glucose metabolism in Duchenne muscular dystrophy: a pet study. *Muscle Nerve* 2002;26:506-12.

87. Cardinal E, Chhem RK, Beauregard CG. Ultrasound-guided interventional procedures in the musculoskeletal system. *Radiol Clin North Am* 1998;36:597-604.

88. Pillen S, Scholten RR, Zwarts MJ, Verrips A. Quantitative skeletal muscle ultrasonography in children with suspected neuromuscular disease. *Muscle Nerve* 2003;27:699-705.

89. Fenster A DD, Cardinal HN. Three-dimensional ultrasound imaging. *Phys Med Biol* 2001;46:R67–99.

90. Bianchi S, Martinoli, C. Ultrasound of the Musculoskeletal System. In: Springer, ed. Diagnostic Imaging. New York: Springer, 2006:50-60.

CHAPTER 2
FUNCTIONAL IMAGING OF DISEASE PROGRESSION IN MURINE MODELS OF DUCHENNE MUSCULAR DYSTROPHY

The contents of this chapter have been adapted from the paper entitled "Functional Imaging of Disease Progression in Murine Models of Duchenne Muscular Dystrophy", submitted to Molecular Imaging (2008) by Ahmad N, Hoffman L, Welch I, Hadway J, Grange R, Dhanvantari S, Chemm R, Hill D, Lee TY.

2.0   INTRODUCTION

As mentioned in chapter one muscle instability in DMD arises due to a loss of dystrophin from the dystrophin-glycoprotein complex (DGC) that links the cytoskeleton with the extracellular matrix and fortifies the integrity of the cell membrane during contraction.[1,2] Contraction-induced damage to the sarcolemma allows cytosolic Ca^{+2} levels to increase, and initiates a cascade of intracellular events that lead to necrosis.[3,4] Lack of dystrophin also leads to a cytosolic mislocalization of the nitric oxide synthase isoform that is normally linked to the DGC in skeletal muscle (nNOS), producing ischemia.[5-7] This, in conjunction with membrane leakage and necrosis, triggers an inflammatory reaction [8] that is typically evidenced through muscle biopsies and histological analyses that reveal necrotic or degenerating muscle fibers surrounded by macrophages and CD4+ lymphocytes. [9] The associated immunological effect is a second source promoting the pathology seen in Duchenne, which if removed may create a milder phenotype.[9]

Family history and PCR genotyping are used to diagnosis DMD, while analysis of disease progression typically relies upon the measurement of strength, creatine kinase

levels and muscle biopsy assessment.[10] To date, there is no effective means to reliably and non-invasively assess the progression of muscle wasting in DMD. Previous studies have reported the use of Magnetic Resonance Imaging (MRI) and its ability to detect change in muscle architecture [11] or difference in muscle permeability [12] in mdx mice, an animal model of DMD. As well studies utilizing positron emission tomography (PET) have attempted to measure differences seen in cardiac metabolism between wild type and mdx mice.[13] However, longitudinal non-invasive imaging studies assessing changes in skeletal musculature perfusion and metabolism remain lacking. In the present study, we demonstrate the utility of using dynamic contrast enhanced CT (DCE-CT) and PET scanning to non-invasively assess the progression of muscle pathogenesis in murine models of DMD.

2.1 MATERIALS AND METHODS

2.1.1 Animal Models of Duchenne Muscular Dystrophy

Wild type (C57BL/6) and mdx (mutated dystrophin) mice were purchased from Charles River and Jackson Laboratories, respectively. Mdx mice were bred with mdx:utrophin heterozygote mice to generate udx mice lacking utrophin and functional dystrophin. Four groups of mice were used for imaging: 1) control wild-type (wt, n=9), which were exercised involuntarily, as described below; 2) exercised mdx (n=9); 3) non-exercised mdx (n=9); and 4) non-exercised udx (n=11). The same four groups with twelve mice in each were used for histology at different times (see histology section below). All protocols were approved by institutional Animal Ethic Committees and conducted according to guidelines set by the Canadian Council on Animal Care.

2.1.2   Exercise and Non-Exercise Protocol

Mdx and wt mice in the exercised group ran 3 times weekly for 30 minutes each time, at a speed of 15 meters per minute (mpm) and a 7-degree (positive) incline on a motorized treadmill (Accuscan Instruments), starting at 6 weeks of age up until 22 weeks of age. To ensure that all animals in the study were handled similarly, non-exercised mdx and udx mice walked on the treadmill 3 times weekly for 10 minutes each time at 5 – 7mpm with no incline. Exercise animals began running 45 minutes before scans; before anesthetic induction, 15 minutes of rest were given to all groups.

2.1.3   CT and PET Imaging

All mice were imaged at 6 weeks of age prior to initiation of either the exercise or the non-exercise protocol and imaged thereafter bi-weekly for another 16 weeks till 22 weeks of age. During each imaging session anesthesia was induced with 3-4% isoflourane and then maintained with 1.5% isofluorane balance oxygen mixture, delivered at a constant rate of 1L/min. All imaging focused on the gastrocnemius muscle of the hind limb because it allowed for more consistent placement of regions of interest (ROI) in longitudinal DCE-CT and PET studies due to its larger size than other muscle groups and hence visibility in those images. As well, the results of each mouse over the course of the longitudinal imaging studies could be normalized with respect to its own baseline to minimize biological variability between different mice.

2.1.4 DCE-CT Scanning for Measurement of Muscle Blood Flow and Blood Volume

A 4 cm thick slab of both hind limbs including the gastrocnemius muscle, separated into forty 0.9 mm thick slices at 175 μm resolution, was scanned repetitively with a GE Healthcare eXplore Locus Ultra μCT scanner. The 5-minute scan duration was divided into two phases: first, 1 s scan for 30 s and then one 1 s scan every 15 s for the remainder of the scan duration. Five seconds into the first phase of scanning, contrast agent (150 μL of diluted Hypaque 300, 200 mg of iodine per ml) was injected via a catheter placed in a tail vein at an injection rate of 2.0 ml/min with an infusion pump (New Era Pump Systems Inc) that was triggered by the CT scanner. CT Perfusion software (GE Healthcare) was used to analyze data. CT Perfusion is based on a modification of the Johnson and Wilson model to describe the exchange of contrast between the blood stream and the interstitial space in terms of blood flow and blood volume.[14,15] These parameters were then used to calculate functional maps of the acquired series of CT images [14] in healthy/degenerating muscle when there is leakage of contrast from the vascular space into the interstitial space.[16] From the derived BF and BV maps, mean BF and BV in gastrocnemius muscles of a CT slice were derived by ROI analysis. Values from all ROI'S of the gastrocnemius in a mouse were weighted according to area and averaged; the averaged values were then normalized by the corresponding baseline values. Finally, results from mice respective to their own group and week were averaged.

2.1.5 PET Scanning for Measurement of Glucose Metabolism

A small dose of a glucose analog, fluorine-18 labeled fluorodeoxyglucose (^{18}F-FDG, 11-38 MBq), was administered via a tail vein. Forty to sixty minutes after injection,

the gastrocnemius muscles in the hind limbs were imaged with a small animal PET scanner (GE Healthcare, eXplore Vista DR), using a photopeak window of 250-700 keV for a duration of 30 minutes. The acquired data were corrected for scatter and reconstructed using an OSEM algorithm into twenty-six 1.7 mm thick slices at a transaxial resolution of 1.6 mm. The (sensitivity) factor for converting counts in reconstructed PET images to activity (in MBq) was determined at regular intervals by scanning with the PET scanner a 5 cm diameter water phantom filled with a known amount of F-18 activity (11-14 MBq), and using the mouse imaging parameters. Regions of interest (ROIs) were drawn in coronal PET slices to encompass the entire gastrocnemius muscle. Values from all ROI's of the gastrocnemius of a mouse were weighted according to area and averaged. The average count for the gastrocnemius muscle was converted into mean activity using the conversion factor determined above, then normalized by the injected activity and the body weight of the animal to arrive at the standardized uptake value (SUV), a semi-quantitative indicator of the average glucose metabolic rate over the period from injection to measurement.[17,18] The SUVs were normalized by the baseline value for each mouse, normalized values were then averaged respective to week and group.

2.1.6 Histological Analysis

Mice used for histology were treated and exercised in the same manner as imaged mice. Twelve extra mice were added to each group for sacrifice at baseline, week 8, 14, and 22 after the beginning of the exercise regime. After sacrifice, the gastrocnemius muscles were dissected from mice in each group and fixed in 10% neutral-buffered

formalin for a minimum of 48 hours. The fixed muscles were embedded in paraffin wax and cut transversely in 5-micron sections and stained with haematoxylin and eosin (H&E).[19] The stained sections were subsequently evaluated for histological features characteristic of DMD such as fiber necrosis, fiber regeneration, hypercontracted fibers, myophagia, macrophagic infiltration, endomysial fibrosis and variability of individual fiber caliber in muscle as dystrophy progresses. Centrally- as opposed to eccentrically-located nuclei are another classic hallmark of the disease and reflect a state in which damaged myofibers initiate repair through the activation, proliferation, self-renewal and differentiation of satellite cells into mature muscle cells.[9,20]

2.1.7 Data Analysis

SPSS Statistics software package for Windows (SPSS Inc., V15.0) was used for statistical operations/analysis. A repeated measures ANOVA was used as an omnibus test to identify significant differences among groups and time points within groups for normalized blood flow, volume, and SUV of F-18 FDG in gastrocnemius muscle. Tukey tests were used for the post-hoc analyses of differences.

2.2. RESULTS

2.2.1 Survival of Mice from the Different Experimental Groups

Figure 2.1 shows the Kaplan Meier survival curves of mice from the four different experimental groups. At the termination of the longitudinal study, 67%, 67%, 56% and 0% of mice from the exercised wt, non-exercised mdx, exercised mdx and non-exercised

udx group survives. There are significant differences in survival between non-exercised
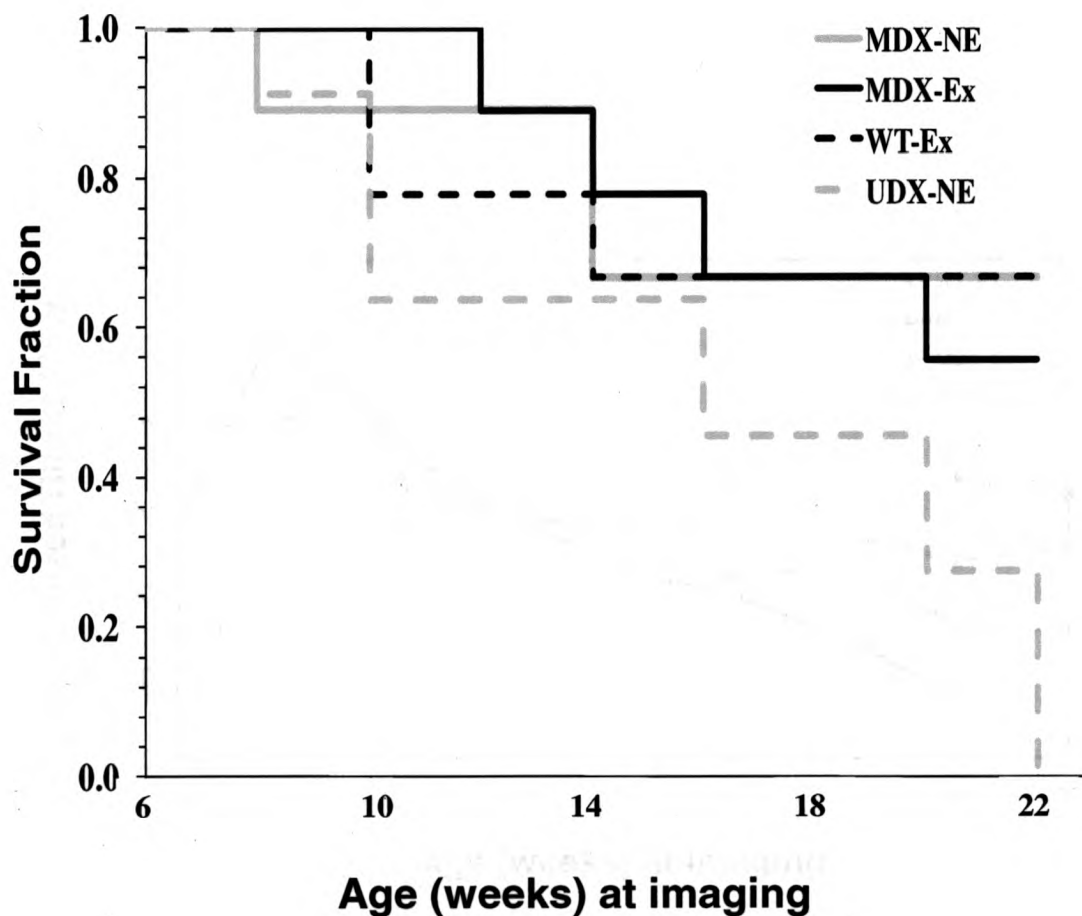
udx and the other three groups of mice.

Figure 2.1. Kaplan Meier survival curves of the four groups of mice used in the longitudinal study after initiation of exercise regime: exercised wild type (WT-Ex), non-exercised mdx (MDX-N.E.), exercised mdx (MDX-Ex) and exercised udx (UDX-Ex). Mice sacrificed at specified histological time points were not included in Kaplan Meier survival curve.

2.2.2 Early Changes in Perfusion, Metabolism and Histology Following Exercise

As illustrated in Fig 2.2, the normalized blood flow and volume in the gastrocnemius muscles of healthy exercised wild type (wt) mice did not change significantly from baseline over time.

. **Figure 2.2a: Perfusion (blood flow) in gastrocnemius muscle over a 14-16 week period in WT and affected mice.** Normalized blood flow in gastrocnemius muscle were collected over a 14-16 week period from age 6 to 20-22 weeks in exercised wt (WT-Ex), non-exercised mdx (MDX-N.E.), exercised mdx (MDX-Ex) and non-exercised udx (UDX-N.E.) mice. Plotted values are means and standard deviations of normalized blood flow for surviving mice from each group. Significant differences ($p<0.05$) were found at age 8 and 20 weeks between: WT-Ex and MDX-N.E. (μ), WT-Ex and MDX-Ex (Ω), WT-Ex and UDX-N.E.(Φ), MDX-N.E. and MDX-Ex (*), MDX-N.E. and UDX-N.E (ψ), MDX-Ex and UDX-N.E (λ).
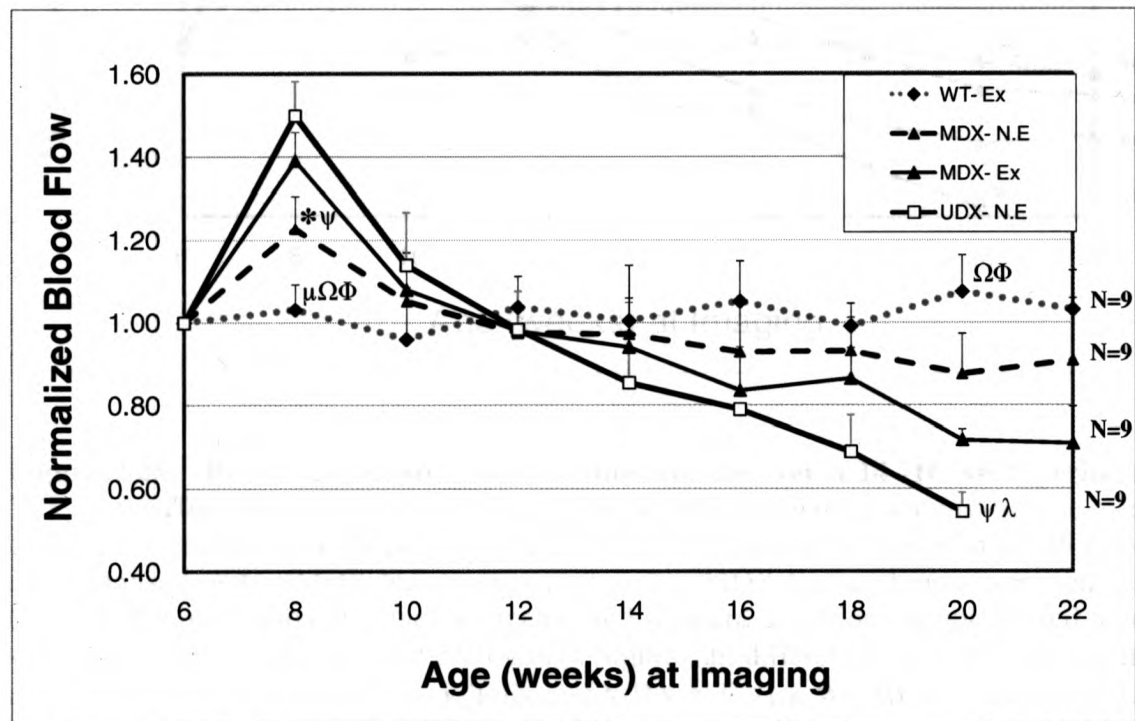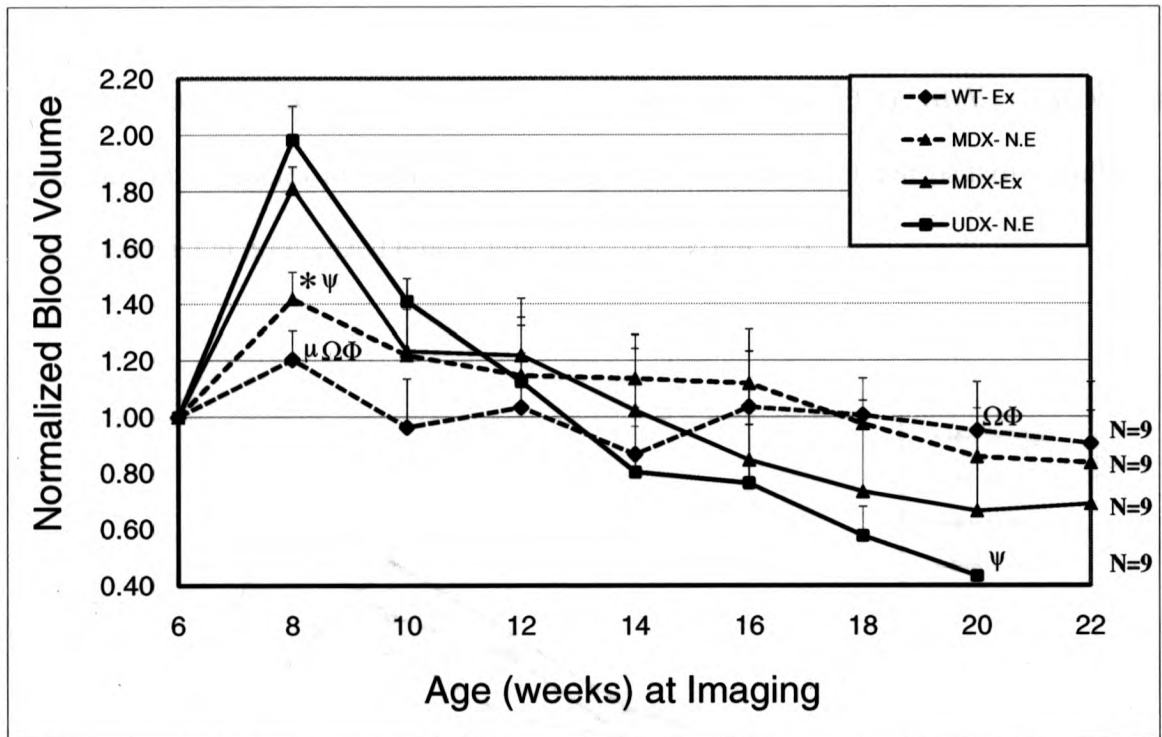
Figure 2.2b: Blood volume in gastrocnemius muscle over a 14 -16 week period in WT and affected mice. Normalized blood volume in gastrocnemius muscle were collected over a 14-16 week period from age 6 to 20-22 weeks in exercised wt (WT-Ex), non-exercised mdx (MDX-N.E.), exercised mdx (MDX-Ex) and non-exercised udx (UDX-N.E.) mice. Plotted values are means and standard deviations of normalized blood volume for surviving mice from each group. Significant differences (p<0.05) were found at age 8 and 20 weeks between: WT-Ex and MDX-N.E. (μ), WT-Ex and MDX-Ex (Ω), WT-Ex and UDX-N.E.(Φ), MDX-N.E. and MDX-Ex (*), MDX-N.E. and UDX-N.E (ψ).

Both normalized blood flow (NBF) and blood volume (NBV) peaked at 8 weeks post baseline in non-exercised mdx, exercised mdx and udx mice. A significant increase in NBF of 18%, 38% and 42%, and for NBV a 40%, 79% and 97% above their respective baseline was detected (P < 0.05), and all NBFs and NBVs were significantly different from those of wt mice (P< 0.05). Additionally, NBFs and NBVs at week 8 between non-

exercised mdx and udx mice and between non-exercised and exercised mdx mice were significantly different (p<0.05).

Glucose uptake as assessed by normalized F-18 FDG SUV (NSUV) in gastrocnemius muscles in each of the four groups of mice exhibited patterns similar to those observed in normalized blood flow and volume (Fig 2.3).
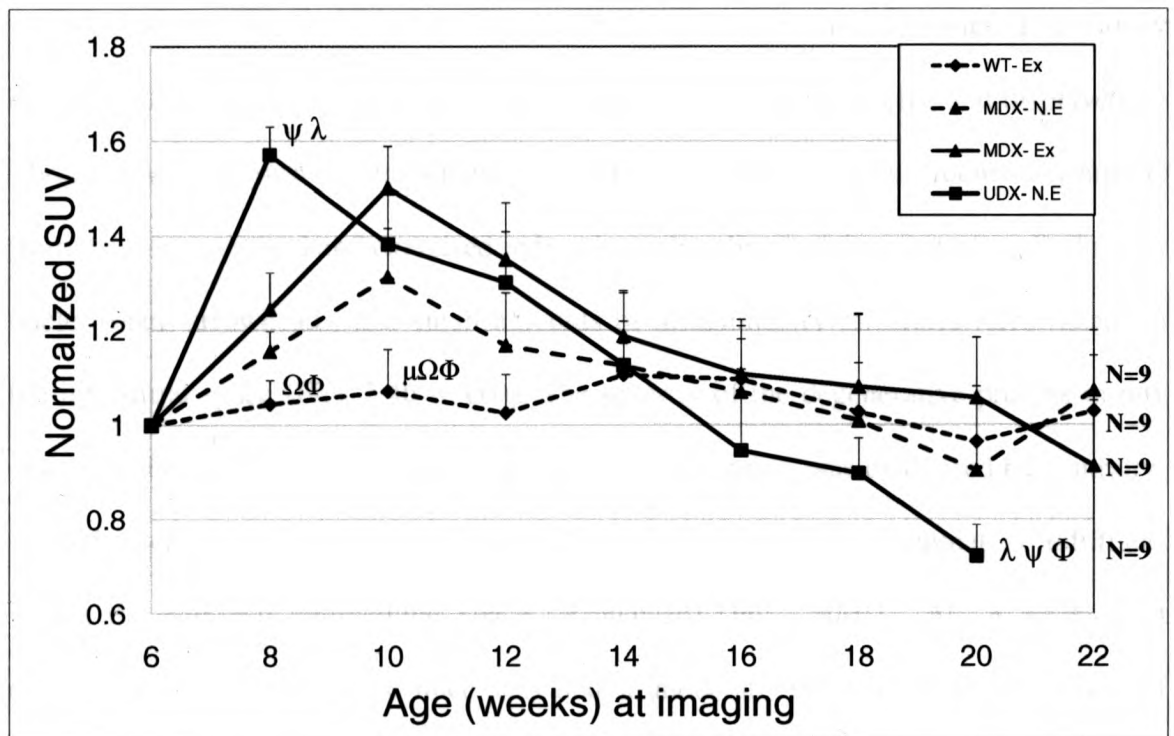
Figure 2.3: SUV of ^{18}F-FDG in gastrocnemius muscle over a 14-16 week period in wt and affected mice. Normalized SUV of ^{18}F-FDG in gastrocnemius muscle were collected over a 14-16 week period from age 6 to 20-22 weeks in exercised wt (WT-Ex), non-exercised mdx (MDX-N.E.), exercised mdx (MDX-Ex) and non-exercised udx (UDX-N.E.) mice. Plotted values are means and standard deviations of normalized SUV of surviving mice from each group. Significant differences (p<0.05) were found at week 8 and 20 between: WT-Ex and MDX-N.E. (μ), WT-Ex and MDX-Ex (Ω), WT-Ex and UDX-N.E.(Φ), MDX-N.E. and MDX-Ex (*), MDX-N.E. and UDX-N.E (ψ), MDX-Ex and UDX-N.E (λ).

NSUVs in non-exercised and exercised mdx mice 10 weeks post-baseline was higher than wt mice ($P < 0.05$) and exhibited a 31% and 50% increase from baselines respectively ($P < 0.05$). NSUV in severely-affected udx mice, in contrast, exhibited a pronounced maximum at 8 weeks post-baseline which was higher than that of the wt mice ($P<0.05$) and represented a 62% increase above its respective baseline ($P<0.05$).

Analysis of H&E stained tissue sections revealed that the gastrocnemius muscle of wt mice at baseline (6 weeks of age), and at all time points thereafter, had mostly eccentrically-located nuclei (arrow), was devoid of inflammatory cells, and displayed no fibrous tissue amongst the myofibers (Fig 2.4a). In contrast, the gastrocnemius muscle from the non-exercised and exercised mdx mice at baseline had frequent centrally-located nuclei (open arrowhead), and small amounts of inflammatory infiltrates (arrowhead) in the interstitial space (Figs 2.4b & c(i)). The severity of the degenerative process in udx mice, relative to that occurring in mildly-affected mdx mice, was evidenced by centrally-located nuclei (open arrowhead) and widespread presence of inflammatory infiltrates within the enlarged intercellular space (arrowhead) (Fig 2.4d(i)). At 8 weeks post exercise, non-exercised mdx mice revealed a moderate increase in the presence of inflammatory infiltrate (arrowhead) amongst the presence of numerous myofibers with centrally-located nuclei (open arrowhead) suggesting active muscle regeneration (Fig 2.4b(ii)). While centrally-located nuclei were also observed in exercised mdx and udx mice (open arrowhead), both groups of mice were characterized by the presence of a marked inflammatory infiltrate amongst necrotic myofibers (Figs 2.4c & d(ii)) and occasional presence of mineralized lesion (Fig 2.4c(ii), arrowhead).

2.2.3 *Intermediate and Late Changes in Perfusion, Metabolism and Histology Following Exercise*

For healthy exercised wt mice, NBF, NBV and NSUV of the gastrocnemius muscle did not change significantly from baseline to 22 weeks of age (Figs 2.2 & 2.3). In the gastrocnemius muscle of non-exercised mdx mice, however, there was a progressive decline in all three imaging biomarkers: NBF (Fig 2.2a), NBV (Fig 2.2b) and NSUV (Fig 2.3) from their respective maximum at 8 weeks of age. Similar, albeit greater, declines in the imaging biomarkers were observed in both exercised mdx mice and non-exercised udx mice. Importantly, both declines of NBF and NBV, particularly at 20 weeks of age (Fig 2.2), accurately reflected the disease state in each model, with mildly-affected mdx mice being intermediate to healthy wt. and severely-affected udx mice; also, a greater decline was noted in exercised compared to non-exercised mdx mice.

These imaging findings again correlated with histological analysis at week 14 and at the termination of our study at 20-22 weeks of age. As illustrated in Fig 4, H&E-stained sections of gastrocnemius muscle taken from either non-exercised or exercised mdx mice at their endpoint revealed that many of the injured myofibers had reverted to eccentrically-located nuclei illustrating healthy myofibers (open arrowhead in Figs 2.4 b & c(iii & iv)). Only a mild inflammatory infiltrate and few necrotic myofibers were observed in these mice, particularly at 22 weeks of age. In udx mice, in comparison, myofibers exhibited atrophy and continued degenerative myonecrosis with an extensive to moderate inflammatory infiltrate (Figs 2.4d (iii & iv).

Figure 2.4a: H&E-stained sections of gastrocnemius muscles isolated from wild type at (i) baseline (6 weeks old), (ii) week 8, (iii) week 14, and at the termination of the study (iv) 20-22 weeks of age. The pathology seen is described in the text. Legend: solid arrow points to eccentrically-located nuclei.
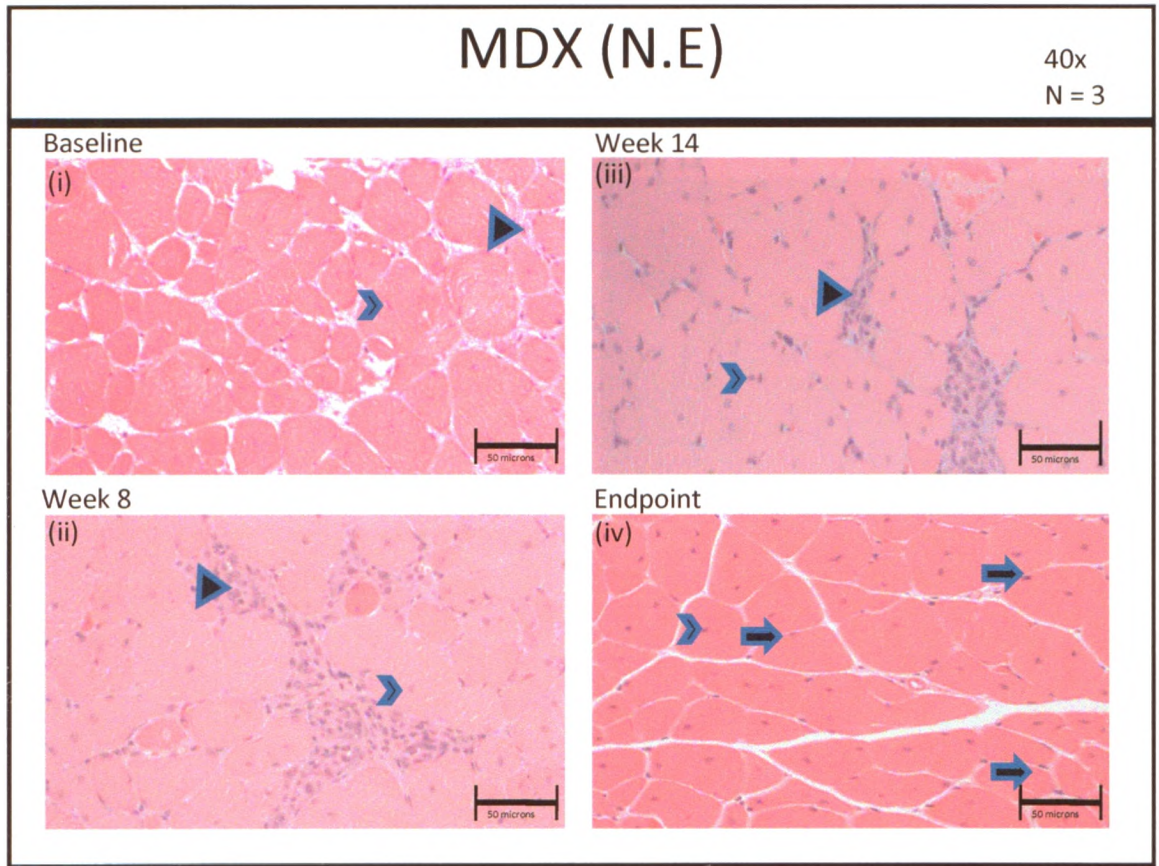
Figure 2.4b: H&E-stained sections of gastrocnemius muscles isolated non-exercised mdx at (i) baseline (6 weeks old), (ii) week 8, (iii) week 14, and at the termination of the study (iv) 20-22 weeks of age. The pathology seen is described in the text. Legend: thin arrowhead points to centrally-located nuclei in muscle fiber; closed arrowhead points to inflammatory infiltrate, solid arrow points eccentrically-located nuclei.
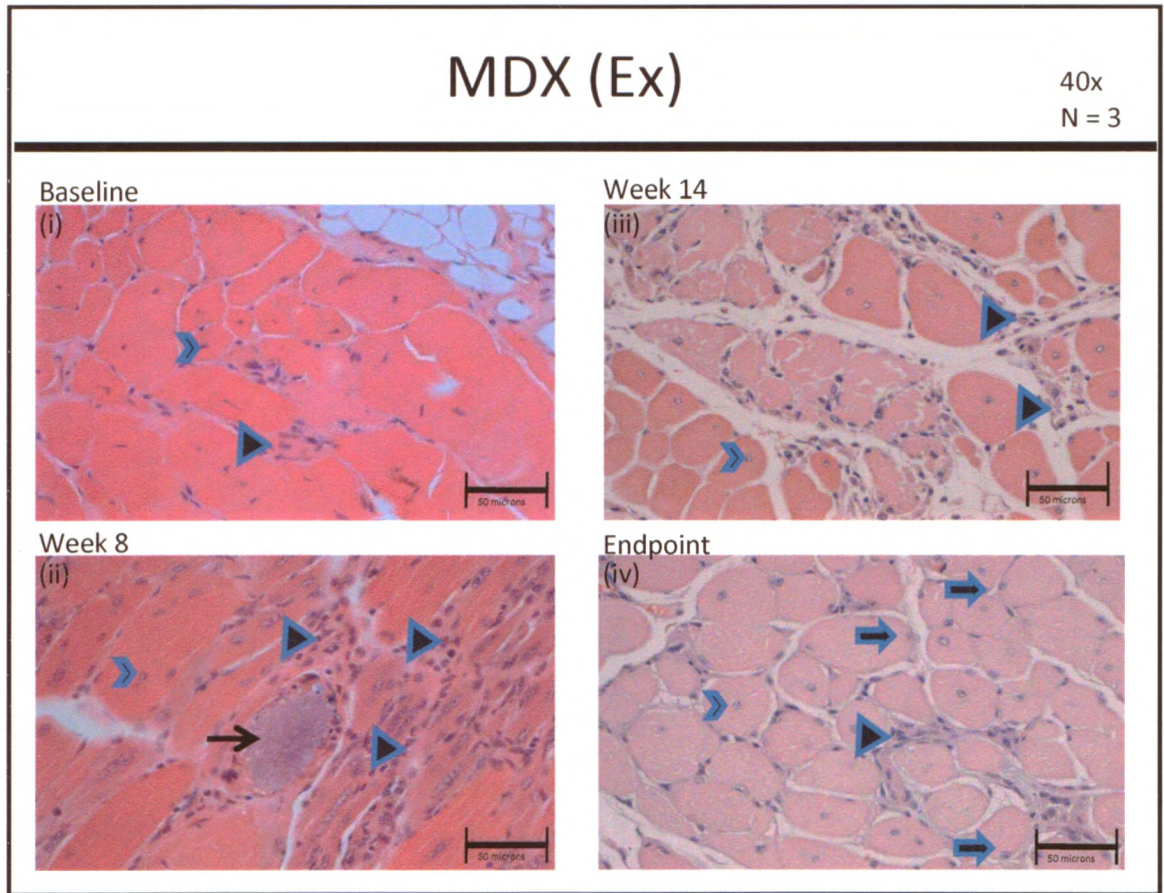
Figure 2.4c: **H&E-stained sections of gastrocnemius muscles isolated from exercised mdx** at (i) baseline (6 weeks old), (ii) week 8, (iii) week 14, and at the termination of the study (iv) 20-22 weeks of age. The pathology seen in each group and at each time are described in the text. Legend: solid arrow points to eccentrically-located nuclei; thin arrowhead points to centrally-located nuclei in muscle fiber; closed arrowhead points to inflammatory infiltrate; and thin solid arrow points to mineralized lesion.
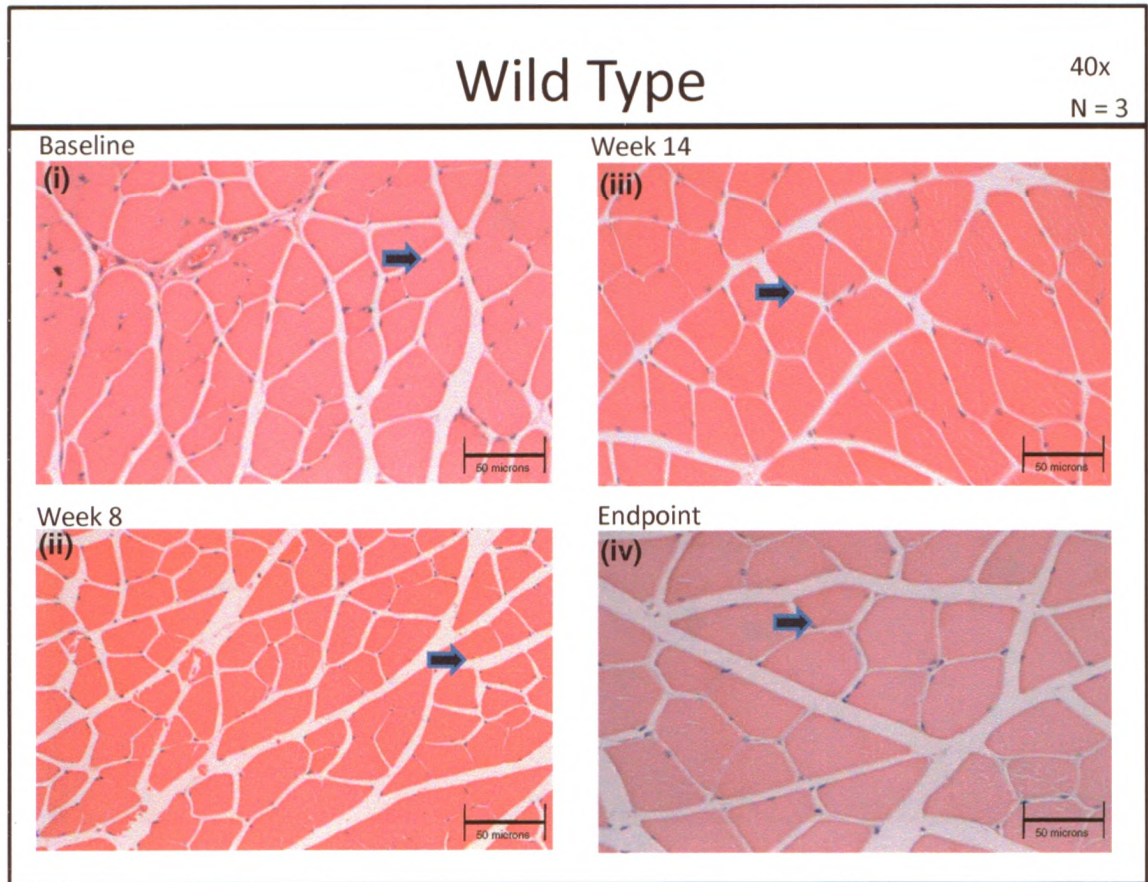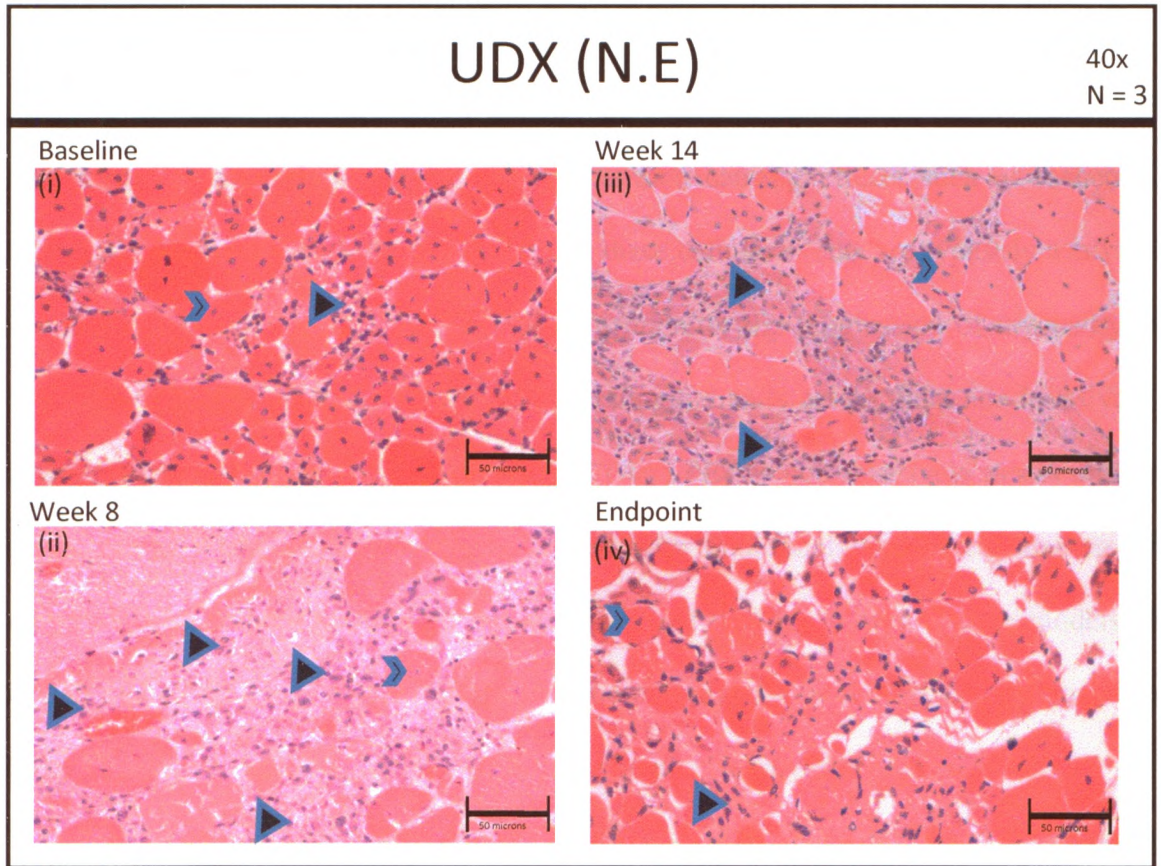
Figure 2.4d: H&E-stained sections of gastrocnemius muscles isolated from udx non-exercise at (i) baseline (6 weeks old), (ii) week 8, (iii) week 14, and at the termination of the study (iv) 20-22 weeks of age. The pathology seen in each group and at each time are described in the text. Legend: solid arrow points eccentrically located nuclei; thin arrowhead points to centrally located nuclei in muscle fiber; closed arrowhead points to inflammatory infiltrate.

2.3   DISCUSSION

Muscle damage in DMD occurs due to the loss of dystrophin.[1,2] This loss results in contraction-induced damage to the sarcolemma causing effects such as ischemia, leucocytic infiltration and necrosis.[3-7] While these cellular events are typically analyzed histologically, their use as effective indices to monitor the progression of myopathy in dystrophic fibers is limited by the inability to longitudinally assess them non-invasively. In the present study, we have utilized DCE-CT and PET to non-invasively assess muscle degeneration. These findings were correlated with traditional histological markers of muscle degeneration/regeneration, inflammation and necrosis. Using murine models of DMD, our study has provided insight into the mechanisms of muscle damage, and the order of events preceding manifestations of myopathy and myofiber necrosis.

Imaging and histological correlation displayed initial stages of increased damage in mdx mice, followed by subsequent healing in later time points of the study, which differs from that seen in humans. However, recent gene expression profiling has displayed overlapping patterns of gene expression between mdx mice and humans.[21] Additionally, recent studies have shown that both sarcolemma stabilization and contractile mechanisms are impaired in muscle from mdx mice.[22] Thus, the mdx mouse still serves as an effective model of DMD, due to similarities in molecular and cellular impairment of muscle function with DMD patients. The mild phenotype of mdx mice is attributed to an up-regulation of utrophin, a homolog of dystrophin which compensates when functional dystrophin is lacking.[23] The udx model displayed much more severity in disease progression, more closely paralleling that seen in DMD patients.[24] Possibly, due to the lack of utrophin to substitute for non-functioning dystrophin, udx mice also do not show

any stages of recovery such as those seen in the mdx model. These severely affected mice continued progressive degeneration with little to no regeneration and resulted in significantly different survival rates in our longitudinal study compared to non-exercised and exercised mdx mice.

Previous reports have shown acceleration of the degenerative-regeneration process in mdx mice through involuntary treadmill running [9] which in turn causes decreased expression of hormones such as IGF-1 and proteins such as Myo-D which may further affect the degenerative state.[25] The exercised mdx mice in our study did exhibit increased myopathy; specifically seen in the exercised mdx group at 8 weeks of age which revealed a greater number of necrotic myofibers and leucocytes, relative to non-exercised mdx mice. In support of these studies, we also observed a transient increase in blood flow, blood volume, and glucose uptake in dystrophic animals at 8 weeks of age. These findings further suggest that the increases observed in perfusion and metabolism reflect the regenerative/repair process that occurs in response to muscle damage and ischemia. However, such a regenerative effort could not be maintained over an extended period, as evidenced by a subsequent progressive decrease in blood flow, blood volume and metabolism in all groups of dystrophic mice beyond the early regenerative phase. In mdx mice, up-regulation of utrophin may temporarily compensates for muscle damage,[26] however, over time continued fiber loss and depletion of the satellite cell population may result in progressive decline in regenerative capabilities of myofibers. The damage to myofibers seen in udx mice is too severe to repair successfully, owing, in part, to the absence of utrophin to compensate for the dystrophin deficiency. The use of udx mice in our studies clearly demonstrates the utility of non-invasive imaging to longitudinally

assess changes in perfusion and metabolism in a second dystrophic model that exhibited a severer degree of pathogenesis compared to the mdx model.

Although the exercise regime used in this study, exacerbated muscle damage in mdx mice. The present study suggests the utility of using DCE-CT and PET scanning to longitudinally assess disease progression in dystrophic mice subjected to disease-modifying treatment in a non-invasive manner. Examining "low-intensity" exercise as a potential therapy for DMD is particularly attractive because it is simple and unlike cell therapeutics, does not require immune suppression or regulatory approval.[27,28] Low intensity exercise also decreases the expression of markers of oxidative stress.[29] Another intriguing possibility is that the adaptation of muscle to exercise may drive the synthesis of growth factors/cytokines that induce proliferation, migration and fusion of transplanted myoblasts in stem cell therapies.[30] Thus, DCE-CT and PET provide promising non-invasive alternatives to muscle biopsies for the assessment of disease progression in DMD that will further allow longitudinal assessment of the efficacy of novel therapeutic treatments for the disease.

2.4 REFERENCES

1. Blake DJ, Weir A, Newey SE, Davies KE. Function and genetics of dystrophin and dystrophin-related proteins in muscle. *Physiol Rev* 2002;82:291-329.

2. Emery AE. The muscular dystrophies. *Lancet* 2002;359:687-95.

3. Alderton JM, Steinhardt RA. How calcium influx through calcium leak channels is responsible for the elevated levels of calcium-dependent proteolysis in dystrophic myotubes. *Trends Cardiovasc Med* 2000;10:268-72.

4. Ruegg UT, Gillis JM. Calcium homeostasis in dystrophic muscle. *Trends Pharmacol Sci* 1999;20:351-2.

5. Rando TA. Role of nitric oxide in the pathogenesis of muscular dystrophies: a "two hit" hypothesis of the cause of muscle necrosis. *Microsc Res Tech* 2001;55:223-35.

6. Sander M, Chavoshan B, Harris SA, Iannaccone ST, Stull JT, Thomas GD, Victor RG. Functional muscle ischemia in neuronal nitric oxide synthase-deficient skeletal muscle of children with Duchenne muscular dystrophy. *Proc Natl Acad Sci U S A* 2000;97:13818-23.

7. Thomas GD, Sander M, Lau KS, Huang PL, Stull JT, Victor RG. Impaired metabolic modulation of alpha-adrenergic vasoconstriction in dystrophin-deficient skeletal muscle. *Proc Natl Acad Sci U S A* 1998;95:15090-5.

8. Spencer MJ, Tidball JG. Do immune cells promote the pathology of dystrophin-deficient myopathies? *Neuromuscul Disord* 2001;11:556-64.

9. Fraysse B, Liantonio A, Cetrone M, Burdi R, Pierno S, Frigeri A, Pisoni M, Camerino C, De Luca A. The alteration of calcium homeostasis in adult dystrophic mdx muscle fibers is worsened by a chronic exercise in vivo. *Neurobiol Dis* 2004;17:144-54.

10. Hess JW, Macdonald RP, Frederick RJ, Jones RN, Neely J, Gross D. Serum Creatine Phosphokinase (Cpk) Activity in Disorders of Heart and Skeletal Muscle. *Ann Intern Med* 1964;61:1015-28.

11. McIntosh LM, Baker RE, Anderson JE. Magnetic resonance imaging of regenerating and dystrophic mouse muscle. *Biochem Cell Biol* 1998;76:532-41.

12. Straub V, Donahue KM, Allamand V, Davisson RL, Kim YR, Campbell KP. Contrast agent-enhanced magnetic resonance imaging of skeletal muscle damage in animal models of muscular dystrophy. *Magn Reson Med* 2000;44:655-9.

13.	Quinlivan RM, Lewis P, Marsden P, Dundas R, Robb SA, Baker E, Maisey M. Cardiac function, metabolism and perfusion in Duchenne and Becker muscular dystrophy. *Neuromuscul Disord* 1996;6:237-46.

14.	Lee TY, Purdie TG, Stewart E. CT imaging of angiogenesis. *Q J Nucl Med* 2003;47:171-87.

15.	T-Y L. Functional CT: Physiological models. *Trends in Biotechnology* 2002;20:S3-S10.

16.	St Lawrence KS, Lee TY. An adiabatic approximation to the tissue homogeneity model for water exchange in the brain: I. Theoretical derivation. *J Cereb Blood Flow Metab* 1998;18:1365-77.

17.	Huang SC. Anatomy of SUV. Standardized uptake value. *Nucl Med Biol* 2000;27:643-6.

18.	Keyes JW, Jr. SUV: standard uptake or silly useless value? *J Nucl Med* 1995;36:1836-9.

19.	Thompson S. Selected histochemical and histopathological methods. Springfield, IL, 1966.

20.	JE Andersson BB, WK Ovalle. Functional regeneration in hind limb skeletal muscle of the mdx mouse. *J Muscle Res Cell Motil* 1998:499–515.

21.	Turk R, Sterrenburg E, de Meijer EJ, van Ommen GJ, den Dunnen JT, t Hoen PA. Muscle regeneration in dystrophin-deficient mdx mice studied by gene expression profiling. *BMC Genomics* 2005;6:98.

22.	Claflin DR, Brooks SV. Direct observation of failing fibers in muscles of dystrophic mice provides mechanistic insight into muscular dystrophy. *Am J Physiol Cell Physiol* 2008;294:C651-8.

23.	Tinsley J, Deconinck N, Fisher R, Kahn D, Phelps S, Gillis JM, Davies K. Expression of full-length utrophin prevents muscular dystrophy in mdx mice. *Nat Med* 1998;4:1441-4.

24.	Deconinck AE, Potter AC, Tinsley JM, Wood SJ, Vater R, Young C, Metzinger L, Vincent A, Slater CR, Davies KE. Postsynaptic abnormalities at the neuromuscular junctions of utrophin-deficient mice. *J Cell Biol* 1997;136:883-94.

25.	Okano T, Yoshida K, Nakamura A, Sasazawa F, Oide T, Takeda S, Ikeda S. Chronic exercise accelerates the degeneration-regeneration cycle and downregulates insulin-like growth factor-1 in muscle of mdx mice. *Muscle Nerve* 2005;32:191-9.

26. Campbell KP, Crosbie RH. Muscular dystrophy. Utrophin to the rescue. *Nature* 1996;384:308-9.

27. Carter GT, Wineinger MA, Walsh SA, Horasek SJ, Abresch RT, Fowler WM, Jr. Effect of voluntary wheel-running exercise on muscles of the mdx mouse. *Neuromuscul Disord* 1995;5:323-32.

28. Dupont-Versteegden EE, McCarter RJ, Katz MS. Voluntary exercise decreases progression of muscular dystrophy in diaphragm of mdx mice. *J Appl Physiol* 1994;77:1736-41.

29. Kaczor JJ, Hall JE, Payne E, Tarnopolsky MA. Low intensity training decreases markers of oxidative stress in skeletal muscle of mdx mice. *Free Radic Biol Med* 2007;43:145-54.

30. Bouchentouf M, Benabdallah BF, Mills P, Tremblay JP. Exercise improves the success of myoblast transplantation in mdx mice. *Neuromuscul Disord* 2006;16:518-29.

CHAPTER 3
HIGH FREQUENCY ULTRASOUND AS A NON-INVASIVE TOOL TO ASSESS DISEASE PROGRESSION IN MURINE MODELS OF DUCHENNE MUSCULAR DYSTROPHY

The contents of this chapter have been adapted from the paper entitled "High Frequency Ultrasound as a Non-invasive Tool to Assess Disease Progression in Murine Models of Duchenne Muscular Dystrophy", submitted to Ultrasound in Medicine (2008) by Ahmad N, Bygrave M, Chemm R, Hoffman L, Welch I, Grange R, Hill D, Lee TY.

3.0   INTRODUCTION

As mentioned in chapter one, (DMD) arises due to a loss of functional dystrophin, a cytoskeletal structural protein, through a mutation in the dystrophin gene.[1] Thereby, compromising sarcolemma integrity,[2,3] and leading to progressive muscle inflammation,[4,5] membrane leakage and myo-fiber degeneration.[6] While diagnosis of DMD is made by family history and genotyping, analysis of disease progression typically relies upon invasive measurements.[7] To date, there is no effective means to reliably and non-invasively assess the progression of muscle wasting in DMD.

Traditional ultrasound analyses of dystrophic muscle in DMD patients have shown that while normal myofiber volume is preserved in early stages of muscle degeneration, there is an increase in muscle echo intensity relative to healthy individuals.[8-10] Similar findings have also been reported in patients with less-severe forms of muscle dystrophy such as Becker and limb-girdle dystrophies; importantly, the observed changes in muscle echo intensity were found to reflect the severity of the disease.[9] Preclinical studies [9,11,12] using ultrasound revealed abnormalities in echo-

intensity associated with the initial stages of clinical manifestation of muscle degeneration in many patients. As well since the severity viewed in ultrasound findings were found to be related to age and clinical stages of disease progression,[9] this imaging modality appears to provide an effective means of non-invasively visualizing structural changes in degenerative muscle.

High Frequency Ultrasound (HFU) (40MHz) holds the potential to track muscle deterioration serially in mouse models of DMD. HFU provides significant backscatter in mice, necessary for the generation of detailed structural and anatomical images and enhanced soft tissue contrast not readily visible at clinical frequencies. We have previously described the ability of HFU to discriminate hyper-echoic lesions in the dystrophic muscle of mdx mice.[13] Motivation for this study originated when differences were noted between the organized speckle pattern of healthy skeletal muscle contrasted with the speckled patterns seen in affected dystrophic muscle of mice. Healthy muscle structure is highlighted by the fibroadipose septa resulting in a characteristic organized, hyper-echoic banding pattern,[14] different from dystrophic muscle which displays disorganization and disruption of the fibroadipose septa possibly due to atrophy, macrophage infiltration, deterioration of myofibers, and calcification.[15] It was hypothesized that the spatial frequencies observed within healthy and unhealthy skeletal muscles in ultrasound images would vary sufficiently to enable a semi-quantitative grading method [16] of discrimination between groups.

To the best of our knowledge, no established validated parameters using HFU exist in the literature regarding DMD. Thus, quantification of the structural appearance of HFU images of the musculature promises to be a promising tool for diagnosis or

measuring changes in muscle damage over time or in response to an intervention. We believe the advances afforded through the use of HFU imaging in preclinical murine models will directly translate to the enhancement of current clinical practices in the assessment of pathologic changes in myotonic diseases.

3.1 MATERIAL AND METHODS

3.1.1 Subjects

Refer to Section 2.1.1 Animal Models of Duchenne Muscular Dystrophy

3.1.2 Exercise and Non-Exercise Protocol

Refer to Section 2.1.2 Exercise and Non-Exercise Protocol

3.1.3 Three-Dimensional Ultrasound Image Acquisition

To obtain baseline scans, all mice were imaged at 6 weeks of age. Animals from each group were subsequently imaged every second week up to 16 weeks by an experienced ultrasonographer. During each imaging session, mice were anaesthetized under an induction level of 3-4% isoflourane:oxygen and then maintained using a 1.5% isofluorane:oxygen mixture; anaesthetic-induced hypothermia was avoided using a heated imaging stage (THM-100, Indus Instruments, Houston, TX) to maintain core temperature at 36°C.

Depilatory hair removal cream (calcium thioglycolate–based) was used on the lower leg and shank of the mice to enhance the contact of the ultrasound probe with the overlying skin above the muscles of interest. Ultrasound coupling gel (Aquasonic 100,

Parker Laboratories, Inc., Fairfield, NJ) was applied to the depilated skin, and a three-dimensional volume scan of the gastrocnemius was acquired by moving the ultrasound probe through a translation parallel to the long axis of the gastrocnemius medial head using multiple two-dimensional images. The right leg of the animals was imaged in a standard supine position with the legs secured such that the medial head of the gastrocnemius was perpendicular to the probe. Ankle, knee, and thigh angles were kept consistently at 45 degrees to standardize the procedure. Imaging was accomplished using the Vevo 770 High Frequency Ultrasound (VisualSonics, Inc., Toronto, Ontario, Canada) scanner.[17] Three-dimensional images were then reconstructed and visualized using Visual Sonics software.[17] The system uses single-element, B-mode imaging, with a 40 MHz center frequency probe that produces 40 μm axial and 80 μm lateral resolutions at a maximum focal depth of 6 mm. Three-dimensional images were reconstructed from the acquired two-dimensional images using software, 3D-Quantify, developed by one of the co-authors [17]. The reconstructed three-dimensional image was displayed in a dynamic cube view format. Sections of the "cube" in different orientations were displayed by moving a 'cut' plane through the three-dimensional ultrasound data interactively to view the different characteristics of the skeletal muscle. Two observers blinded to the source of the ultrasound images, separately graded images according to a scoring system described below. Any differences between scores were resolved by a collaborating radiologist also blinded to the ultrasound images.

3.1.4 Grading and Scoring System

The scoring system for muscle damage was based on the following characteristics in the HFU images of the gastrocnemius muscle in the right leg: 1) Number of hyper-echoic lesions: discernable points that were more hyper-echoic compared to the surrounding muscle tissue and were not related to the fibroadipose septa were counted. 2) Lesion diameter: long axis diameters were measured using the embedded ultrasound software analysis tool in the Vevo 770 scanner. Visible lesions were given the following values: a value of "1" was assigned to lesions that range from 1-50 μm, "2" to lesions that ranged from 51-100 μm, "3" to lesions that ranged from 101-150 μm, and "4" to lesions that were greater than 151 μm in diameter. 3) Myofiber disorganization: normal muscle organizes myofibers and endomysial connective tissue in a regular repeating pattern that gives rise to the appearance of evenly-distributed hyper-echoic 'streaks' and 'bands' throughout the gastrocnemius. Thus, analysis of myofiber disorganization is based on the disappearance of the regular banding pattern observed in healthy skeletal muscle. More specifically, a value of "0" is assigned to mice that display anisotropic banding, a value of "3" to mice that exhibit moderate skeletal muscle disorganization, and a value of "6' to mice with marked disorganization. Values for lesion number, lesion diameter and myofiber disorganization were summed to give a final damage score, which was used to grade overall myofiber degeneration: 1- none (score 1-4), 2 - minor (score 5-10), 3 - mild (score 11-14), 4 - moderate (score 15-20), 5 - marked (score 21+).

3.1.5   Histological Analyses

Mice used for histology were treated and exercised in the same manner as imaged mice; twelve extra mice were added to each group for sacrifice at specified time points: baseline (6 weeks) and week 8, 14, and 20-22 after the beginning of the exercise regime. The gastrocnemius muscles were dissected from a minimum of 3 mice in each group at each of the time points.   Muscles were fixed in 10% neutral-buffered formalin for a minimum of 48 hours. The fixed muscles were embedded in paraffin wax and cut transversely in 5-micron sections and stained with haematoxylin and eosin (H&E).[18] Comparisons of a minimum of three muscles with similar pathology were taken from each group and time point. Representative H&E slides were then compared with HFU scores as an indication for grades of degeneration. The presence of features seen in the HFU image such as calcified lesions, macrophage infiltration, fat, degeneration of endomysium, and/or changes in banding pattern from fibroadipose septa were examined.

3.1.6   Data Analyses

Statistical analyses were performed using the SPSS Statistics software package for Windows (SPSS Inc., v V15.0). A repeated measure ANOVA was used as an omnibus test to identify significant differences among groups and time points within groups for HFU scores. Tukey tests were used for the post-hoc analyses of differences.

3.2   RESULTS

3.2.1   *Significant Differences in Muscle Health Were Found Between Wild-Type and Affected Animals*

All dystrophic mice developed hyper-echoic lesions in HFU images. Fig 3.1

depicts differences in lesion size and number within an HFU image of the gastrocnemius.

Figure 3.1: B-mode HFU transverse images of a hind limb from 3 dystrophic mice displaying differences in lesion number and size. G- gastrocnemius, S- soleus; A) A 375 µm lesion within the gastrocnemius of a non-exercised udx mouse at week 14. B) Three visible lesions with the largest 120 µm in size within the gastrocnemius of an exercised mdx mouse at week 14. C) Five lesions with the largest 55 µm in size within the gastrocnemius of a non-exercised mdx mouse at week 14.

Based on the overall muscle grade derived from the scores for the 3 parameters of

muscle damage, we observed significant differences in the gastrocnemius muscle

between wt and dystrophic animals (Fig 3.2). However, udx (N.E.) mice were found to

display greater degeneration than either mdx groups (Fig 3.2). Muscle degeneration in

mdx mice peaked at a mild level (grade 2-3) over the course of the study at week 12-14

post exercise and thereafter a non-significant trend of improvement was noted. In

contrast, muscle degeneration in udx mice was progressive and stabilized at grade 4

(moderate) from week 12 to 18 post exercise. After which deterioration to a marked

degree (grade 5) at week 20 was shown, contributing to the death of all udx mice beyond week 20.
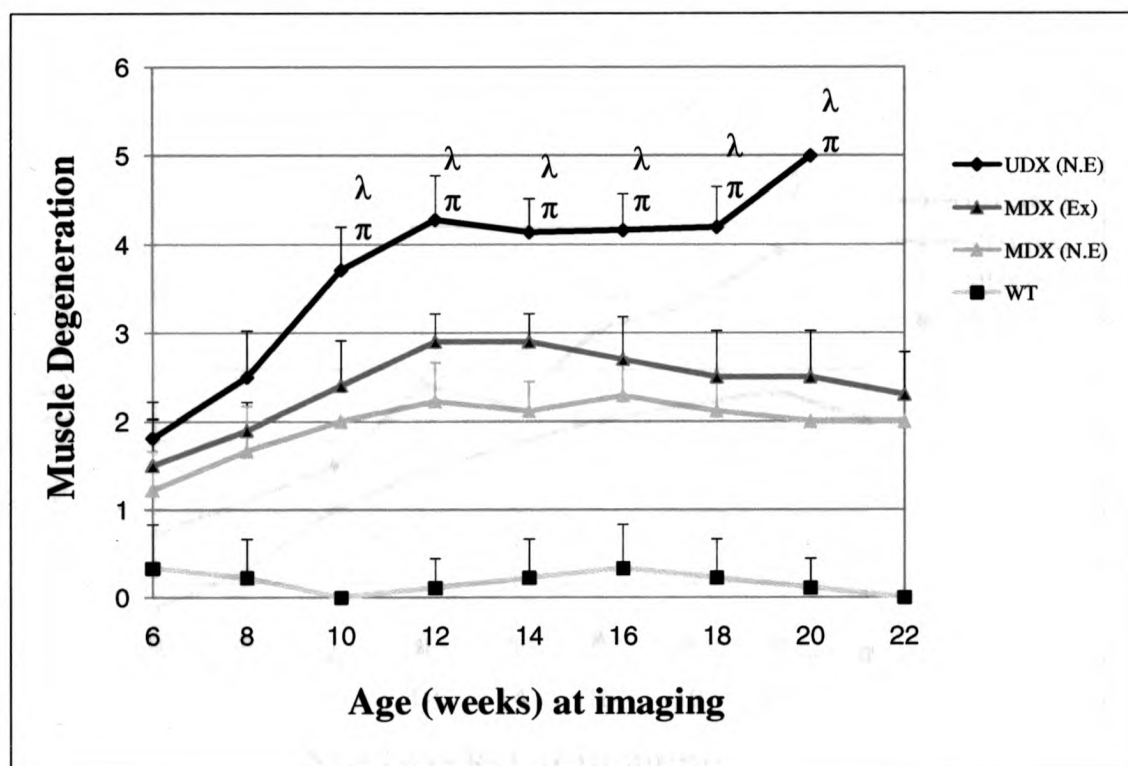

Figure 3.2: Grades of muscle degeneration derived from the sum (mean ±SD) of the three parametric scores over 16 weeks of HFU imaging: 1 = none, 2 = minor, 3 = mild, 4 = moderate, 5 = marked. UDX reached a moderate (4) to marked (5) grade of muscle damage, while mdx both Ex and N.E only reached minor (2) to mild (3) muscle damage. Wild type animals displayed no muscle degeneration (grade < 1) throughout the study. Significant differences (p<0.05) are represented by π between mdx (N.E.) and udx (N.E.), and λ between mdx (Ex) and udx (N.E.).

For each group of mice the number of lesions and the largest lesion diameter were averaged for all mice in respective groups over the time course of the study and plotted in Figs 3.3 and 3.4, respectively. Lesion numbers were greater (p>0.05) in dystrophic animals compared to wt animals from week 8 onwards (Fig 3.3). Udx mice show the highest number of lesions over the course of the study, while no difference was found

between mdx groups. However, udx (N.E) mice showed significantly higher numbers of lesions compared to mdx (N.E) mice and mdx (Ex) mice from week 12 and 18 onwards respectively.
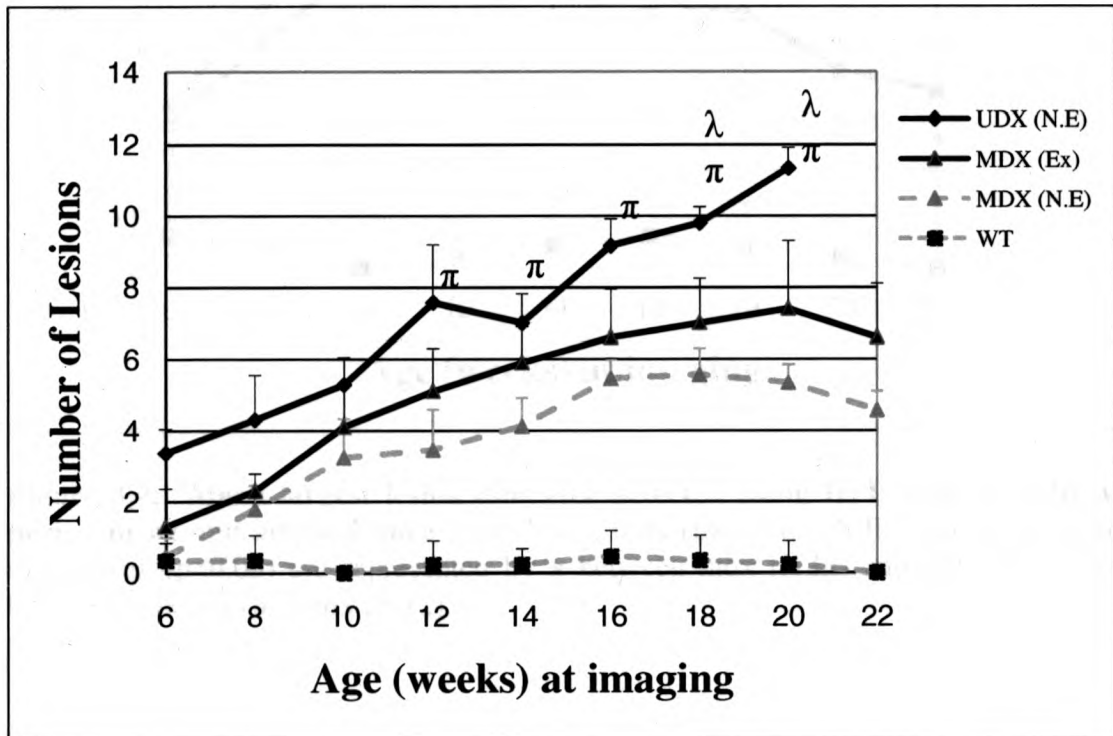
Figure 3.3: Mean number of lesions in gastrocnemius muscle over the time course of the study for each group: udx (N.E.), mdx (Ex), mdx (N.E.) and wt. Significant differences (p<0.05) are represented by π between mdx (N.E.) and udx (N.E.), and λ between mdx (Ex) and udx (N.E.).

Lesion diameter of dystrophic mice increased significantly relative to wt animals (p>0.05) from week 8 onwards. While a significant increase in lesion diameter was observed in udx mice compared to mdx mice from week 14 onwards, no significant differences were found between mdx (N.E) and mdx (Ex) mice. (Fig 3.4)

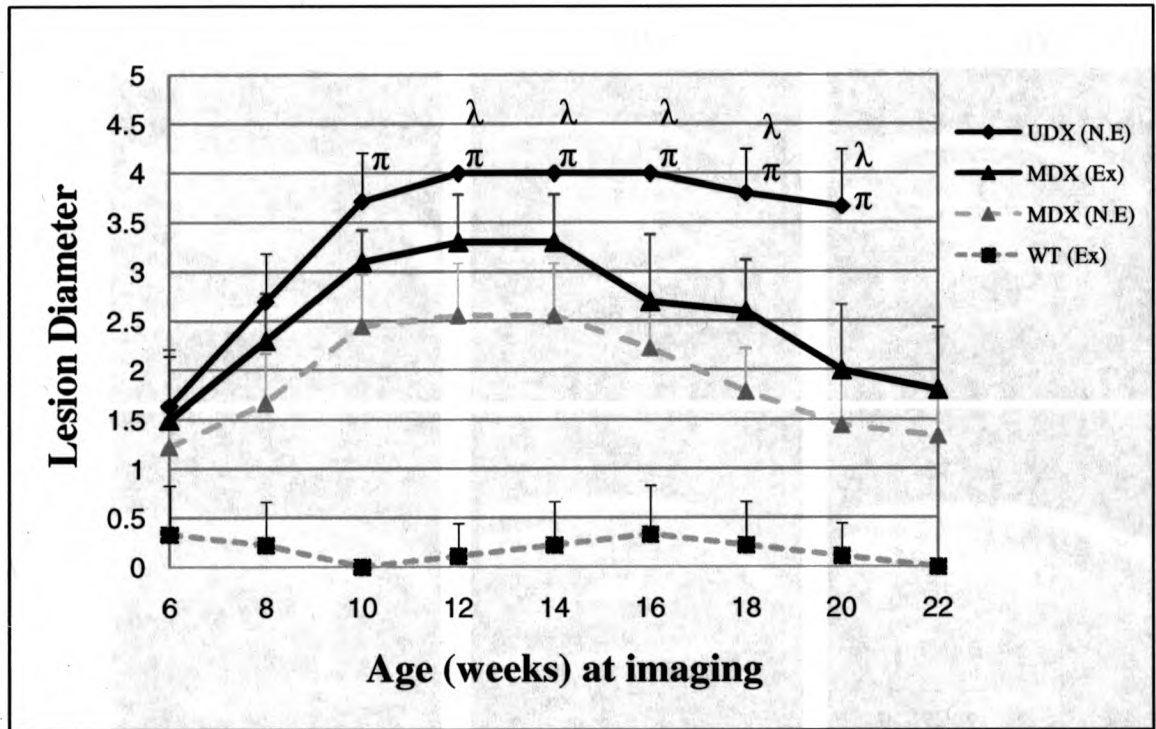**Figure 3.4: Mean largest lesion diameter detected using HFU over a 14-16 week period in wt and affected mice**: udx (N.E.), mdx (Ex), mdx (N.E.) and wt. Significant differences (p<0.05) are represented by π between mdx (N.E.) and udx (N.E.), and λ between mdx (Ex) and udx (N.E.).

Fibroadipose septa in the muscles of wt animals appeared organized resulting in multiple parallel linear echoes visible in HFU images of the gastrocnemius muscle (Figs 3.5A and D); these normal muscle fibers had a disorganization score of 0 for all weeks (Fig 3.6). Both mdx groups displayed some initial disorganization at week 8 (Fig 3.5B), but by the end of the study organization similar to that seen in wt animals were noted (Fig 3.5E). Udx mice showed disorganization from baseline which continually increased in severity till the end-point of the study (Figs 3.5C and F). For each group of mice the disorganization scores were averaged for all the mice in the group over the time course of the study and plotted in Fig 3.6.
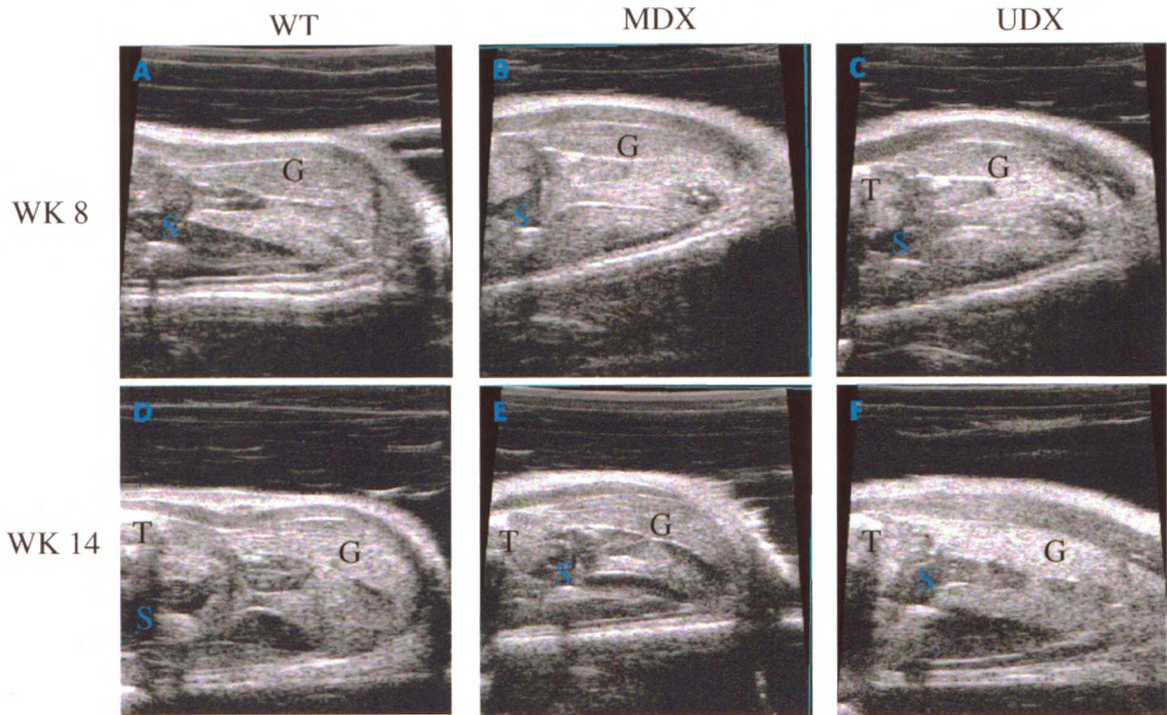
	WT	MDX	UDX

Figure 3.5: B-mode images of muscle disorganization in gastrocnemius muscle at weeks 8 and 14 in wt and affected mice. HFU transverse images of a hind limb from a wild type, a mdx (Ex) and a udx mice at week 8 and 14 post start of exercise regimen. G = Gastrocnemius, S = Soleus, T = Tibia. Comparison of muscle disorganization based on ultrasound echoes from fibroadipose septa: A,D) wt; B,E) mdx (Ex); C,F)udx.

Wild type mice showed no histological changes and all the nuclei were peripherally located (solid arrows) amongst the four selected time points (weeks 6, 8, 14, 20-22 from start of exercise regimen) (Fig 3.7A (i, ii, iii, iv)). N.E. mdx mice displayed initial damage/regeneration at baseline with centrally located nuclei (open arrowhead) and small infiltrate of macrophage (closed arrowhead) (Fig 3.7B i) present. Images from week 8, Fig 3.7B (ii) showed disruption of the endomysium (open arrow), and moderate infiltrate (closed arrowhead), typically seen prior to the formation of calcified lesions. At week 14 myofibers remained in a state of regeneration with centrally located nuclei (open
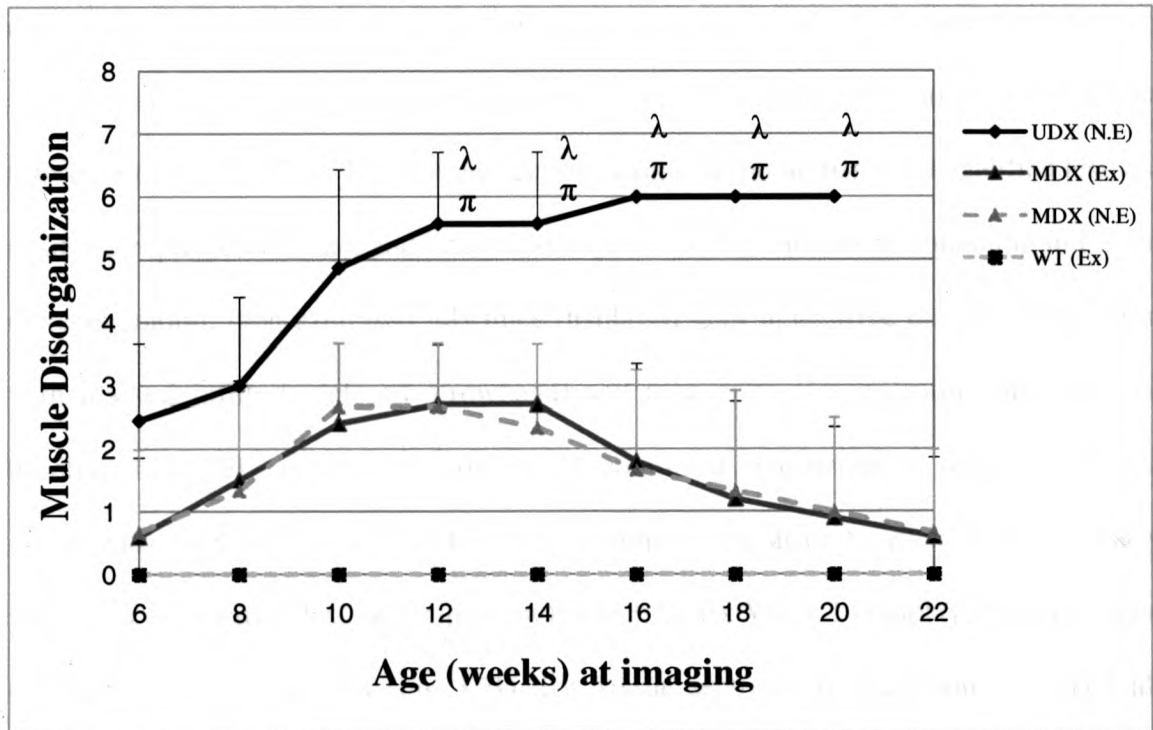
Figure 3.6: Mean disorganization scores of the gastrocnemius muscle over the time course of the study for each group: udx (N.E.), mdx (Ex), mdx (N.E.) and wt. Significant differences (p<0.05) are represented by π between mdx (N.E.) and udx (N.E.), and λ between mdx (Ex) and udx (N.E.).

arrowhead), a moderate influx of macrophage (closed arrowhead), and presence of calcified lesions (thin arrow) (Fig 3.7B iii). At the endpoint, there was little to no infiltration of macrophage (closed arrowhead) and some nuclei have reverted back to a peripheral position (solid arrow), as observed in wt mice, indicating repair, while other myofibers remained in a state of regeneration (open arrowhead). Endomysium of myofibers appeared intact. Exercised mdx mice displayed initial damage at baseline (Fig 3.7C i). Week 8 displayed marked inflammation (closed arrowhead), centrally located nuclei suggesting ongoing regeneration (open arrowhead), scare or calcified lesions (thin arrow), and disruption of the endomysium (open arrow). (Fig 3.7C ii). At week 14,

calcified lesions (thin arrow) as well as mild infiltrate (open arrowhead) were present, centrally located nuclei remained dominant in spite of a few peripherally located nuclei (closed arrow) (Fig 3.7C iii). Tissue sections from end-point displayed calcified lesions, mild macrophage infiltrate, and intact endomysium with some fibers remaining in a state of regeneration. Non-exercised udx mice displayed very aggressive disease progression with marked infiltrate (closed arrowhead) and regenerating/degenerating myofibers at baseline (Fig 3.7D i). Week 8 displayed continued degeneration, infiltrate (closed arrowhead), and disruption of the endomysium (open arrow), as well as the early formation of calcified lesions (thin arrow) (Fig 3.7D ii). Week 14 displayed the presence of macrophage and lesions (Fig 3.7D iii). Tissue sections from endpoint revealed all myofibers remained in a state of regeneration/degeneration (open arrowhead), leucocytic infiltrate remains (black arrow), and extensive endomysium degeneration was noted (open arrow). (Fig 3.7D iv).

3.3   DISCUSSION

The purpose of this study was to demonstrate the ability of using HFU imaging to non-invasively assess muscle degeneration in murine models of DMD. To achieve this, a grading system was developed to classify and quantify the degree of muscle damage observed in HFU images. Two murine models of DMD were selected for comparison, the mdx and udx models. To exacerbate muscle damage in the mdx model; a less severe model of DMD, a subgroup of these mice were subjected to an involuntary treadmill running regime. Our findings demonstrate that HFU can discriminate between animal

Figure 3.7a: H&E-stained sections of gastrocnemius muscles isolated from WT mice at (i) baseline (6 weeks old), (ii) week 8, (iii) week 14 and at the termination of the study (iv) 20-22 weeks of age. The pathology seen is described in the text. Legend: solid arrow points eccentrically located nuclei.

MDX (N.E)   40x   N = 3

Figure 3.7b: H&E-stained sections of gastrocnemius muscles isolated non-exercised mdx mice at (i) baseline (6 weeks old), (ii) week 8, (iii) week 14 and at the termination of the study (iv) 20-22 weeks of age. The pathology seen is described in the text. Legend: open arrowhead points to centrally located nuclei in muscle fiber; closed arrowhead points to inflammatory infiltrate, open arrow points to endomysium disruption, closed arrow points to eccentrically located nuclei, thin arrow points to mineralized lesions.
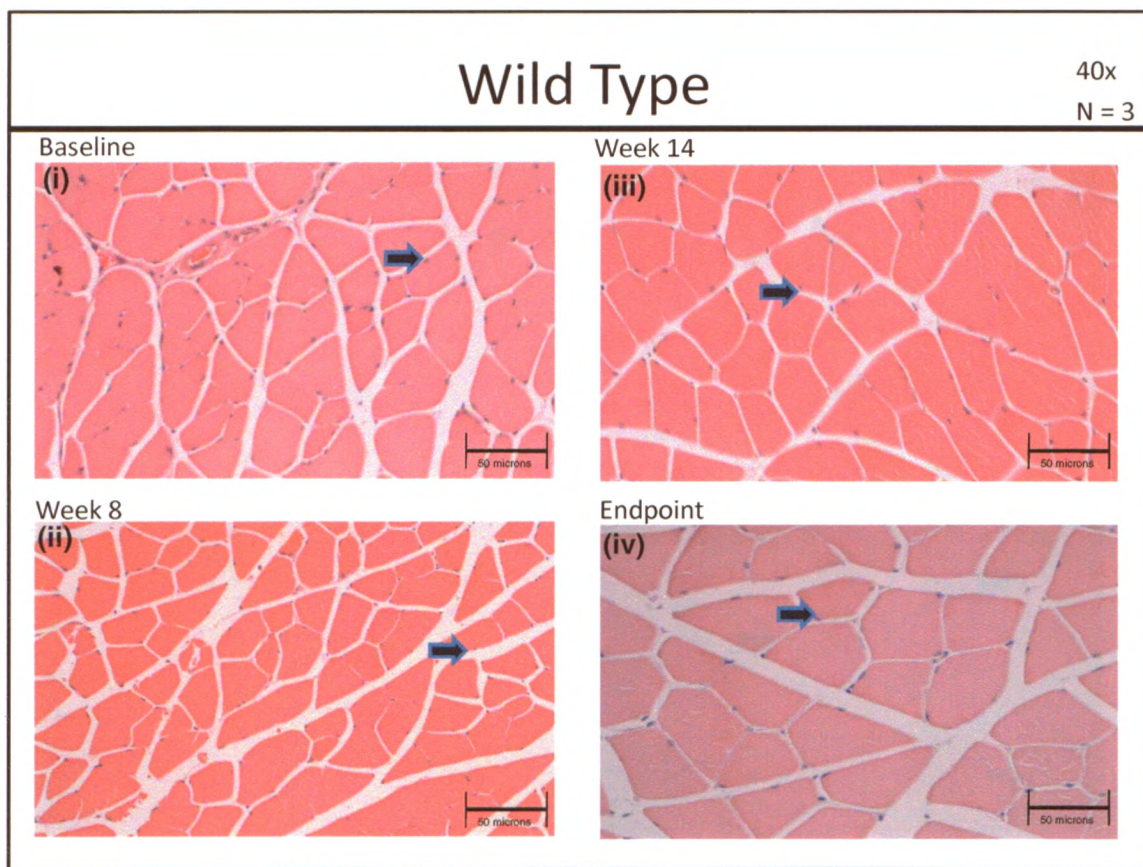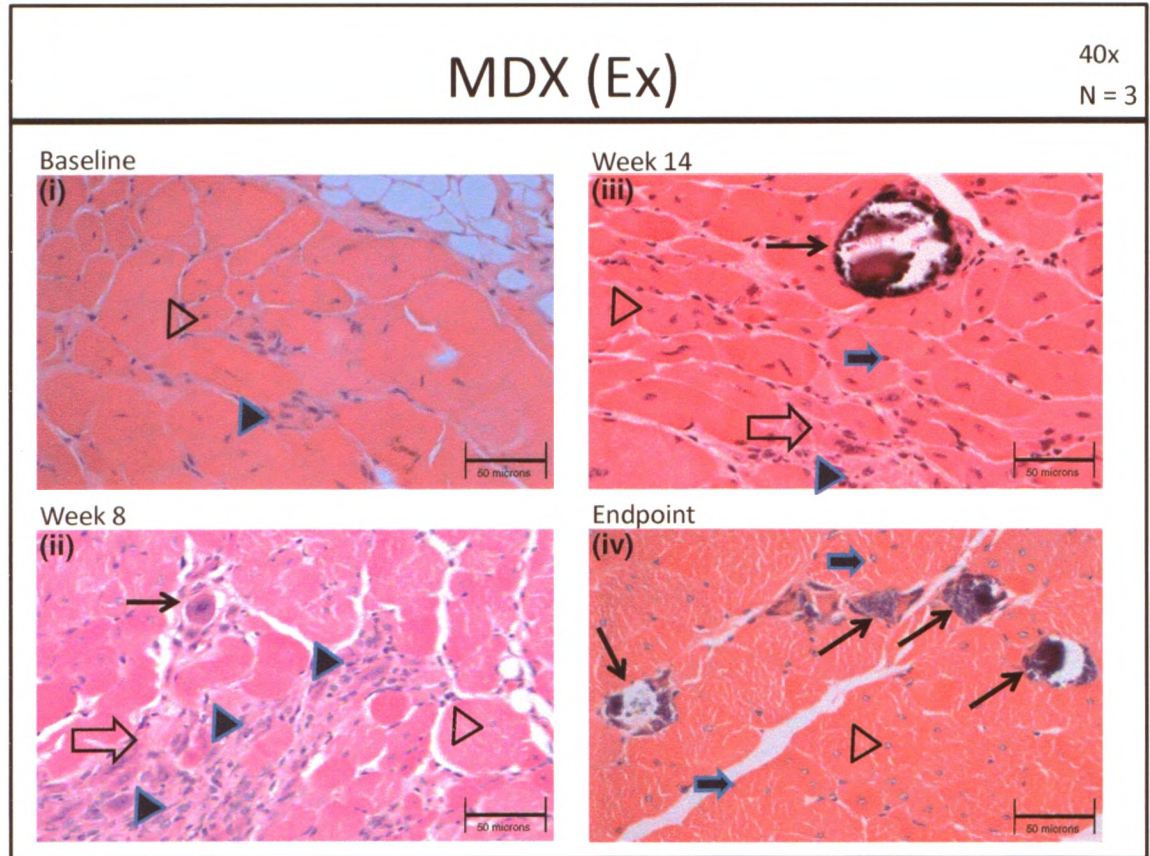
Figure 3.7c: H&E-stained sections of gastrocnemius muscles isolated exercised mdx mice at (i) baseline (6 weeks old), (ii) week 8, (iii) week 14 and at the termination of the study (iv) 20-22 weeks of age. The pathology seen is described in the text. Legend: open arro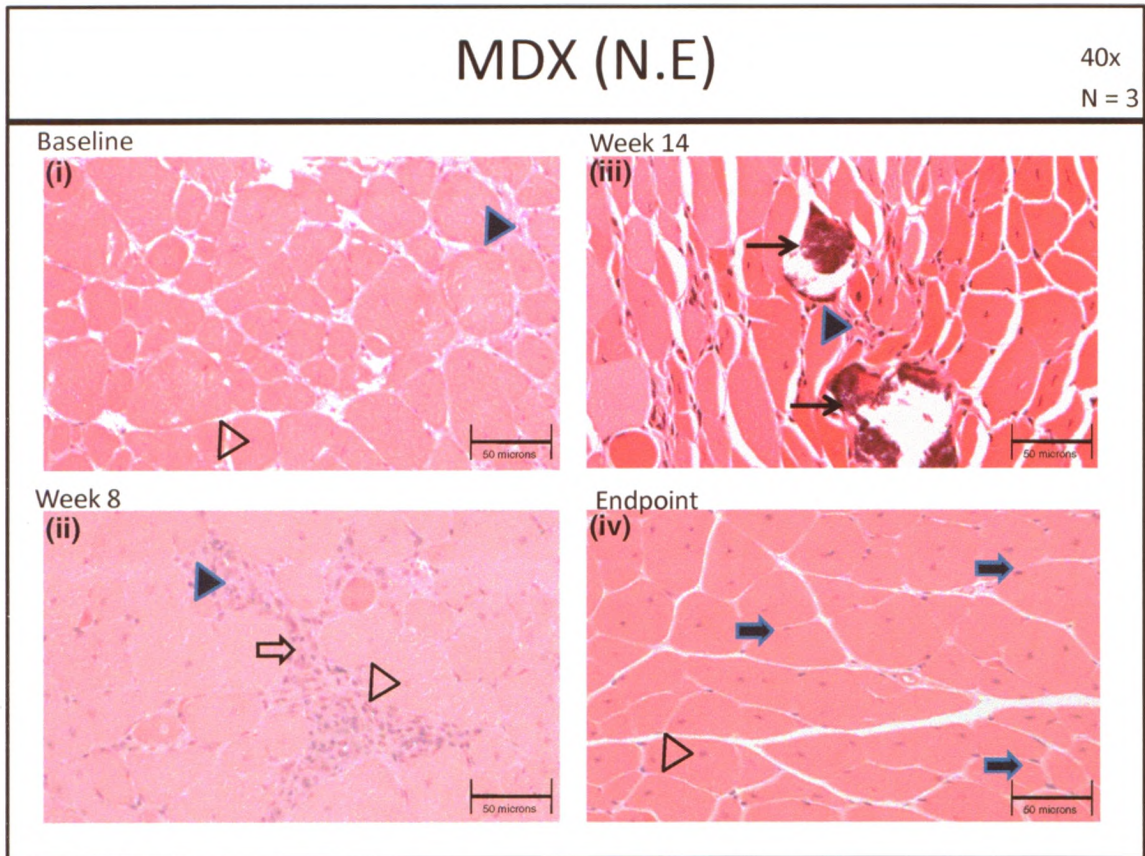whead points to centrally located nuclei in muscle fiber; closed arrowhead points to inflammatory infiltrate, open arrow points to endomysium disruption, closed arrow points to eccentrically-located nuclei, thin arrow points to mineralized lesions.
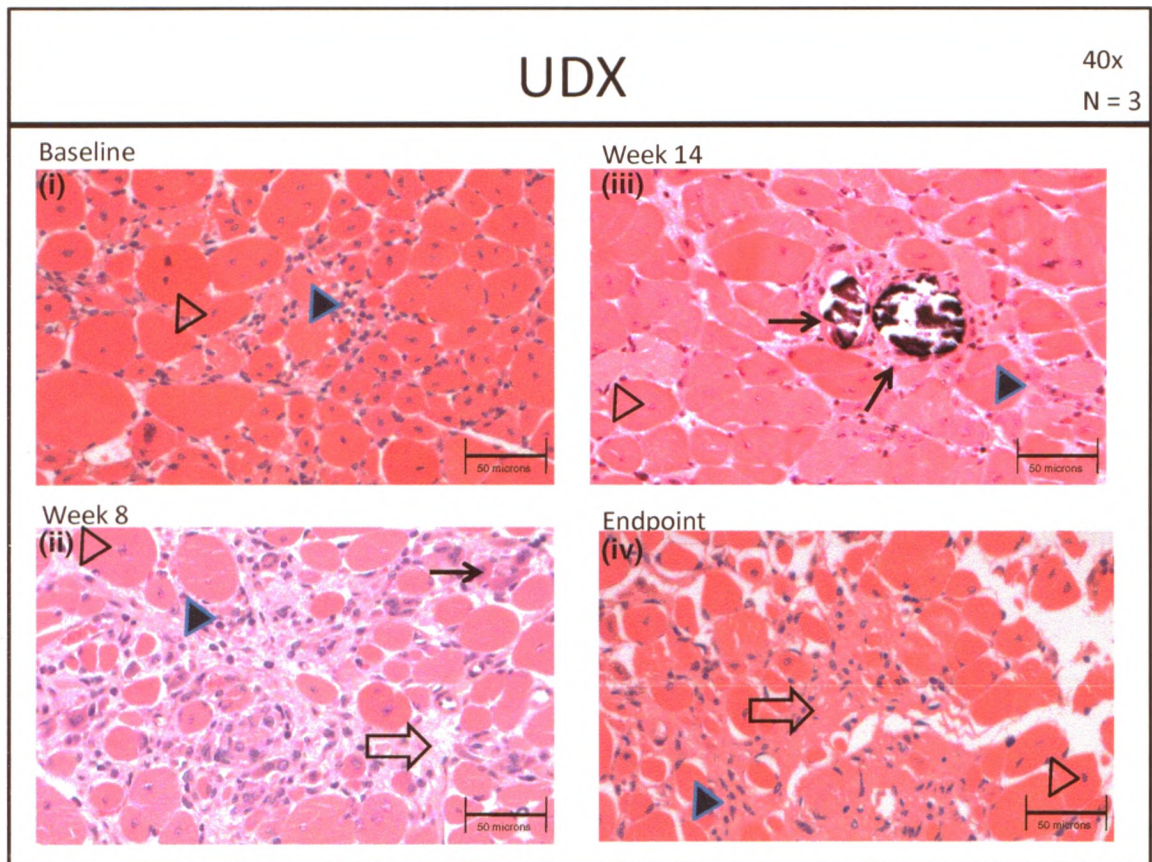
Figure 3.7d: H&E-stained sections of gastrocnemius muscles isolated from udx non-exercise mice at (i) baseline (6 weeks old), (ii) week 8, (iii) week 14 and at the termination of the study (iv) 20-22 weeks from the start of exercise regimen. The pathology seen in each group and at each time are described in the text. Legend: open arrowhead points to centrally located nuclei in muscle fiber; closed arrowhead points to inflammatory infiltrate, open arrow points to endomysium disruption, thin arrow points to mineralized lesions.

models of DMD that exhibit varying degrees of severity, and importantly, can accurately track degenerative changes occurring in muscle throughout the duration of the study. HFU, at the frequency of 40 MHz used in this study, can theoretically resolve groups of hypertrophic myofibers,[19] consisting of small functional groups of muscle cells having undergone substantial dystrophic changes and potentially calcification. Additional changes in the normal echoic speckle pattern of myofiber organization can be caused by an increase or decrease in reflectance due to biomechanical strain or an increase in cellularity.[14,15,20] In our study, these changes were assessed to define a scoring system for muscle damage.

Discrete lesions seen on HFU images of dystrophic mice were either aggregation of infiltrating leucocytes [6,21,22] or calcified necrosis of myofibers.[13] Mdx mice revealed early stages of degeneration with macrophage infiltration in histological sections of the gastrocnemius muscle.[6] The absence of functional dystrophin promotes muscle instability by increasing contraction-induced damage to the sarcolemma allowing cytosolic Ca^{+2} levels to increase.[23,24] This initiates a cascade of intracellular events that lead to necrosis.[23,24] In our histological study, there were dense regions of macrophage accumulation and calcification around degenerative myofibers.

Elevated $[Ca^{2+}]$ in dystrophic muscle has previously been noted [25] and has been attributed to persistently activated calcium channels which are incorporated into the sarcolema membrane during repair.[26] It has been suggested that with continual activation of calcium channels, calcium loading within the myocyte results in myonecrosis and tissue calcification.[26] We believe the accretion of macrophage around calcified lesions in

damaged muscle fibers, followed by macrophage withdrawal may explain changes in the size of lesions seen in mdx mice with HFU. With increasing macrophage infiltration and calcification a lesion observed by HFU may be perceived as having a larger diameter compared to lesions only having macrophage present or calcified scar tissue. The proposed explanation is supported by our histology data on mdx mice. We observed an early macrophage infiltration from initial damage which was followed by up-regulation of utrophin leading to an increase in muscle stability and reduction in myofiber necrosis,[27] and macrophage infiltration. In udx mice, as the utrophin gene is knocked-out, the stabilization effect from utrophin up-regulation is lost. Thus, persistent muscle damage and macrophage infiltration are present after birth in this model contributing to a continual increase in number and size of lesions.

Muscle disorganization was scored according to the visibility of the linear echo banding pattern produced by the normal organization of fibroadipose septa in gastrocnemius muscle. Studies have shown that ultrasound has the capability to assess damage in muscle based on fibroadipose septa organization.[14] Mdx mice in comparison to wt showed more muscle disorganization in the initial weeks due to damage. However, with healing/restoration from up-regulation of utrophin, mdx mice displayed patterns more similar to wt in later weeks of the study. Udx mice showed very little organization in the hyper-echoic banding pattern from baseline and with time more progressive degeneration was evident. Our histology data as well as others suggest that groups of degenerative myofibers, endomysium disruption, fat/collagen deposit and/or macrophage infiltration may all contribute to the hyper-echogenicity seen in the udx and to a lesser extent the mdx mice.[28,29]

In conclusion, HFU images soft tissue in mice at high contrast and spatial resolution thereby demonstrating that this micro-imaging modality has the capability to assess architectural changes in muscle fibers in murine models of DMD. Using our scoring and grading system on HFU images, we were able to assess a higher degree of muscle damage/degeneration in udx than mdx mice, which was corroborated by our histology data. To the best of our knowledge, this is the first study to longitudinally track muscle degeneration using HFU in two murine models of DMD and demonstrate the ability of HFU to differentiate not only between wild type and between disease models of DMD, but within disease models. The grading scheme also holds promise for application in pre-clinical therapeutic trials to monitor treatment affects.

3.4 REFERENCES

1. Hoffman EP, Brown RH, Jr. and Kunkel LM: Dystrophin: the protein product of the Duchenne muscular dystrophy locus. Cell. 51: 919-28, 1987.

2. Blake DJ, Weir A, Newey SE and Davies KE: Function and genetics of dystrophin and dystrophin-related proteins in muscle. Physiol Rev. 82: 291-329, 2002.

3. Emery AE: The muscular dystrophies. Lancet. 359: 687-95, 2002.

4. Bell CD and Conen PE: Histopathological changes in Duchenne muscular dystrophy. J Neurol Sci. 7: 529-44, 1968.

5. Bradley WG and Fulthorpe JJ: Studies of sarcolemmal integrity in myopathic muscle. Neurology. 28: 670-7, 1978.

6. Spencer MJ and Tidball JG: Do immune cells promote the pathology of dystrophin-deficient myopathies? Neuromuscul Disord. 11: 556-64, 2001.

7. Hess JW, Macdonald RP, Frederick RJ, Jones RN, Neely J and Gross D: Serum Creatine Phosphokinase (Cpk) Activity in Disorders of Heart and Skeletal Muscle. Ann Intern Med. 61: 1015-28, 1964.

8. Fischer AQ, Carpenter DW, Hartlage PL, Carroll JE and Stephens S: Muscle imaging in neuromuscular disease using computerized real-time sonography. Muscle Nerve. 11: 270-5, 1988.

9. Heckmatt JZ, Leeman S and Dubowitz V: Ultrasound imaging in the diagnosis of muscle disease. J Pediatr. 101: 656-60, 1982.

10. Heckmatt JZ, Pier N and Dubowitz V: Assessment of quadriceps femoris muscle atrophy and hypertrophy in neuromuscular disease in children. J Clin Ultrasound. 16: 177-81, 1988.

11. Heckmatt JZ, Pier N and Dubowitz V: Real-time ultrasound imaging of muscles. Muscle Nerve. 11: 56-65, 1988.

12. Pillen S, Verrips A, van Alfen N, Arts IM, Sie LT and Zwarts MJ: Quantitative skeletal muscle ultrasound: diagnostic value in childhood neuromuscular disease. Neuromuscul Disord. 17: 509-16, 2007.

13. Ahmad N, Bygraves M, Lee TY and Fenster A: Imaging Findings of Muscular Lesions in Myotinic Murine Models of DMD using High Frequency Ultrasound. J Ultrasound Med. 27: 234, 2008.

14. Bianchi S, Martinoli C, Abdelwahab IF, Derchi LE and Damiani S: Sonographic evaluation of tears of the gastrocnemius medial head ("tennis leg"). J Ultrasound Med. 17: 157-62, 1998.

15. Bianchi S, Martinoli, C.: Ultrasound of the Musculoskeletal System, in Springer: *Diagnostic Imaging.* New York, Springer, 2006, pp 50-60.

16. Meng C, Adler R, Peterson M and Kagen L: Combined use of power Doppler and gray-scale sonography: a new technique for the assessment of inflammatory myopathy. J Rheumatol. 28: 1271-82, 2001.

17. Fenster A DD, Cardinal HN: Three-dimensional ultrasound imaging. Phys Med Biol 46: R67–99, 2001.

18. Thompson S: *Selected histochemical and histopathological methods.* Springfield, IL, 1966.

19. Foster FS, Zhang MY, Zhou YQ, Liu G, Mehi J, Cherin E, Harasiewicz KA, Starkoski BG, Zan L, Knapik DA *et al.*: A new ultrasound instrument for in vivo microimaging of mice. Ultrasound Med Biol. 28: 1165-72, 2002.

20. Koh ES and McNally EG: Ultrasound of skeletal muscle injury. Semin Musculoskelet Radiol. 11: 162-73, 2007.

21. Gosselin LE and McCormick KM: Targeting the immune system to improve ventilatory function in muscular dystrophy. Med Sci Sports Exerc. 36: 44-51, 2004.

22. Holt PG: Down-regulation of immune responses in the lower respiratory tract: the role of alveolar macrophages. Clin Exp Immunol. 63: 261-70, 1986.

23. Alderton JM and Steinhardt RA: Calcium influx through calcium leak channels is responsible for the elevated levels of calcium-dependent proteolysis in dystrophic myotubes. J Biol Chem. 275: 9452-60, 2000.

24. Ruegg UT and Gillis JM: Calcium homeostasis in dystrophic muscle. Trends Pharmacol Sci. 20: 351-2, 1999.

25. Petrof BJ: Molecular pathophysiology of myofiber injury in deficiencies of the dystrophin-glycoprotein complex. Am J Phys Med Rehabil. 81: S162-74, 2002.

26. Elsherif L, Huang MS, Shai SY, Yang Y, Li RY, Chun J, Mekany MA, Chu AL, Kaufman SJ and Ross RS: Combined deficiency of dystrophin and beta1 integrin in the cardiac myocyte causes myocardial dysfunction, fibrosis and calcification. Circ Res. 102: 1109-17, 2008.

27. Tinsley J, Deconinck N, Fisher R, Kahn D, Phelps S, Gillis JM and Davies K: Expression of full-length utrophin prevents muscular dystrophy in mdx mice. Nat Med. 4: 1441-4, 1998.

28. Cullen MJ, Mastaglia F.l.: *Pathological reactions of skeletal muscle. In: Mastaglia FL, Walton JN (eds) Skeletal muscle pathology.* Edinburgh, Churchill Livingstone, 1982, pp 88 - 139.

29. Cullen MJ and Jaros E: Ultrastructure of the skeletal muscle in the X chromosome-linked dystrophic (mdx) mouse. Comparison with Duchenne muscular dystrophy. Acta Neuropathol. 77: 69-81, 1988.

CHAPTER 4
CONCLUSIONS AND FUTURE WORK

4.0   SUMMARY

The primary objective of this thesis was to investigate muscle degeneration in two murine models of DMD using three non-invasive imaging modalities; DCE-CT, PET, and HFU. Each modality assessed complimentary aspects of muscle degeneration. DCE-CT assessed changes in blood flow and blood volume, PET assessed changes in metabolism and HFU characterized changes in muscle architecture over a 16 week period from 6 weeks of age. A strong correlation was demonstrated between these non-invasive modalities and histology revealing pathogenetic causes of muscle degeneration in the murine model.

The next sections summarize results of each experiment completed in this thesis, followed by a discussion of the experimental and clinical relevance of all major findings. Although we were successful in accurately tracking changes in muscle degeneration using the three imaging modalities, further research is required before the full clinical potential of the technique is realized. Appropriately, this chapter also discusses future directions of research in the application of techniques developed.

4.1   FUNCTIONAL IMAGING OF DISEASE PROGRESSION IN MURINE MODELS OF DUCHENNE MUSCULAR DYSTROPHY

Chapter 2 presents the results of using two functional non-invasive imaging modalities to assess DMD; DCE-CT and PET. Two transgenic murine models were utilized, the mildly affected mdx model and the severely affected udx model. Disease

progression in both models was followed over 16 weeks by assessing changes in blood flow (BF), blood volume (BV) and metabolism of skeletal muscle. A subgroup of mdx mice was exercised in order to exacerbate muscle damage in the hope of being able to detect novel changes from their non-exercised counterpart. Non-exercised mdx and udx mice were imaged and assessed similarly as the exercised mdx mice. An increase in normalized BF, BV, and metabolism in the gastrocnemius muscle was observed in earlier weeks post-baseline in non-exercised mdx mice. The increase was even greater in exercised mdx mice and greater still in the more severely affected udx mice relative to wt mice. Intermediate to late weeks displayed a progressive decline in affected animals for all three imaging biomarkers from the maximum at two weeks post exercise. Similar, albeit greater, declines in the imaging biomarkers were observed in both exercised mdx mice and non-exercise udx mice. Importantly, both normalized BF and BV accurately reflected the disease state in each model, with decreases from the maximum in mildly affected mdx mice being intermediate to healthy wt and severely affected udx mice.

4.2   THREE-DIMENSIONAL ULTRASOUND MICROIMAGING TO GRADE DISEASE PROGRESSION IN TRANSGENIC MURINE MODELS OF DUCHENNE MUSCULAR DYSTROPHY

Chapter 3 presents the results of a study using High Frequency Ultrasound (HFU) to detect muscular architectural changes occurring in two mouse models of muscular dystrophy. Mice were exercised in a similar manner as the study in Chapter 2. Muscle architecture was scored using three parameters 1) lesion number 2) lesion diameter and 3) muscle organization, scores of each were accumulated and the degree of degeneration was graded as: 1 none, 2 minor, 3 mild, 4 moderate, 5 marked. Udx mice were shown to begin with mild (3) to moderate (4) degeneration/damage at baseline and continual

disease progression was noted over the duration of the study; by the end of the study, all udx animals showed grade 5 (marked) muscle damage. Hyperechogenicity as noted in the udx model can occur due to an increase in the number of acoustic interfaces. This may have been generated by fat accumulation, fibrosis, degeneration of endomysium and inflammation. Furthermore, the homogeneous rather than the striated appearance of muscle may be due to the loss/disruption of fibroadipose septa, histologically these features were noted. Both mdx mice groups (exercised and non-exercised) began with close to no damage, HFU imaging at intermediate time points revealed moderate (4) structural damage, while endpoint assessment revealed regeneration and scored mild damage (3). Initial signs of leucocytic infiltration and myonecrosis were noted, however no substantial accumulation of fat, fibrosis or endomysium degeneration were noted at the end of the study.

4.3   EXPERIMENTAL AND CLINICAL RELEVANCE

The studies completed in this thesis have a number of implications experimentally. The techniques developed provide methods of measuring underlying dystrophic changes in more than one animal model with more than one imaging modality. Additionally, these modalities can be used repeatedly for longitudinal studies due to the non-invasive nature of experiments. Longitudinal studies with regular non-invasive assessments are crucial as they allow researchers to quantify trends within each individual animal. Traditionally, methods of measuring disease progression in muscular dystrophy are considerably more invasive and provide limited functional information per measurement. Another experimental implication of this study is that a number of

imaging modalities can be combined to maximize information on prognosis and pathological progression. With this said, the imaging methods presented in this thesis are far from being used in clinical applications. These preliminary studies were done as a prerequisite for future therapeutic studies in mice. Before any clinical applications can be considered the study must be repeated in larger mammals more physiologically similar to humans such as dogs or pigs. However the relevant information discovered was that muscle blood flow, blood volume and SUV of F-18 labeled fluorodeoxyglucose are potential imaging markers for muscle degeneration in muscular dystrophy. As well HFU can be used to detect architectural changes in degenerative muscle. These in turn can be used as alternatives to muscle biopsies and blood serum creatine kinase levels as non-invasive markers to monitor disease progression and treatment responses in DMD.

4.4   FUTURE WORK

The present studies demonstrate the potential of using DCE-CT, PET and HFU scanning to longitudinally assess disease progression in skeletal muscle of dystrophic mice. Continuing along this path DECT, PET and HFU should be used to further assess functional parameters in cardiac and brain tissue in dystrophic mouse models, as degenerative processes are continually occurring in these organs. Furthermore, therapeutic regimens such as "low-intensity" exercise as a potential therapy for DMD is particularly attractive because it is simple and unlike cell therapeutics, does not require immune suppression or regulatory approval.[1,2] Low intensity exercise also decreases the expression of markers of oxidative stress.[3,4,5] Another intriguing possibility is that the adaptation of muscle to exercise may drive the synthesis of growth factors/cytokines that

induce proliferation, migration and fusion of transplanted myoblasts in stem cell therapies.[6] Thus, these technologies provide a promising non-invasive alternative to muscle biopsies for the assessment of disease progression that will further allow us to longitudinally assess the efficacy of various therapeutic treatments for DMD.

4.5 LIMITATIONS

There are several limitations in our study. Each DCE-CT and PET scan gave ~ 26 mSv of radiation dose to the mouse bi-weekly. Since overt muscle damage was not seen in the wt mice, primary radiation damage in the dystrophic mice can be ruled out. However, the additive effect of radiation on ischemic and inflammatory effects to exacerbate damage seen in the dystrophic mice is a possible confounding factor. In addition, clinically end stage mortality occurs due to cardio/respiratory failure. Induction of isoflourane for approximately 1 hour bi-weekly for 16 weeks may have accelerated vasomodulatory and respiratory defects causing premature death.

4.6 CONCLUSIONS

The most significant findings of this thesis are listed below:

1) The DCE-CT and PET methods of measuring BF, BV and SUV were demonstrated to be sensitive enough to differentiate muscle degeneration between wild type, non-exercised mdx, exercised mdx mice and non-exercised udx mice.

2) DCE-CT and PET are capable of providing non-invasive imaging markers for muscle degeneration in muscular dystrophy.

3) HFU was able to discriminate between wild type, mdx and udx animals based on degenerative changes in muscle architecture. As well soft tissue contrast is sufficient to detect the presence of inflammatory infiltrates, calcified lesions, and fibroadipose septum disruption in dystrophic muscle.

4.7 REFERENCES

1. Carter GT, Wineinger MA, Walsh SA, Horasek SJ, Abresch RT, Fowler WM, Jr. Effect of voluntary wheel-running exercise on muscles of the mdx mouse. *Neuromuscul Disord* 1995;5:323-32.

2. Dupont-Versteegden EE, McCarter RJ, Katz MS. Voluntary exercise decreases progression of muscular dystrophy in diaphragm of mdx mice. *J Appl Physiol* 1994;77:1736-41.

3. Kaczor JJ, Hall JE, Payne E, Tarnopolsky MA. Low intensity training decreases markers of oxidative stress in skeletal muscle of mdx mice. *Free Radic Biol Med* 2007;43:145-54.

4. Ansved T. Muscular dystrophies: influence of physical conditioning on the disease evolution. *Curr Opin Clin Nutr Metab Care* 2003;6:435-9.

5. Grange RW, Call JA. Recommendations to define exercise prescription for Duchenne muscular dystrophy. *Exerc Sport Sci Rev* 2007;35:12-7.

6. Bouchentouf M, Benabdallah BF, Mills P, Tremblay JP. Exercise improves the success of myoblast transplantation in mdx mice. *Neuromuscul Disord* 2006;16:518-29.

Western

June 28, 2004

This is the Original Approval of this protocol
*A Full protocol submission will be required in
2008

Dear Dr. Lee:

Your "Application to Use Animals for Research or Teaching" entitled:

"CT Measurement of Sarcolemmal Permeability as an Early Indicator of Muscle Degeneration in MDX
Mice"
Funding Agency-- Intra-Mural

has been approved by the University Council on Animal Care. This approval is valid from June 28, 2004 to May
31, 2005. The protocol number is # 2004-061-06.

1. This number must be indicated when ordering animals for this project.
2. Animals for other projects may not be ordered under this number.
3. If no number appears please contact this office when grant approval is received.
   If the application for funding is not successful and you wish to proceed with the project, request that an
internal scientific peer review be performed by the Animal Use Subcommittee office.
4. Purchases of animals other than through this system must be cleared through the ACVS office. Health
certificates will be required.

ANIMALS APPROVED   FOR 1 YR.   Pain Level - C

    Mice   - MDX   3-4 wks M   -   5
           - C57 Bl 3-4 wks M   -   10

STANDARD OPERATING PROCEDURES
Procedures in this protocol should be carried out according to the following SOPs. Please contact the
Animal Use Subcommittee office (661-2111 ext. 86770) in case of difficulties or if you require copies.
SOP's are also available at http://www.uwo.ca/animal/acvs
        # 310 Holding Period Post Admission
        # 320 Euthanasia
        # 321 Criteria for Early Euthanasia/Rodents

REQUIREMENTS/COMMENTS
Please ensure that individual(s) performing procedures on live animals, as described in this protocol, are
familiar with the contents of this document.

c.c. Approved Protocol   -   T.Y. Lee, J. Hadway, D. Forder
     Approval Letter   J. Hadway, D. Forder

University Council on Animal Care • The University of Western Ontario
Animal Use Subcommittee • Health Sciences Centre • London, Ontario • N6A 5C1 • Canada